Exit of human cutaneous resident memory CD4 T cells that enter the circulation and seed distant skin sites

M. M. Klicznik[1]†, P. A. Morawski[2]†, B. Höllbacher[1,2], S. R. Varkhande[1], S. Motley[2], M. D. Rosenblum[3], S. A. Long[2], G. Brachtl[4], T. Duhen[2], D. J. Campbell[2,5]*‡, I. K. Gratz[1,2,6]*‡

[1] Department of Biosciences, University of Salzburg, Salzburg, Austria.

[2] Benaroya Research Institute, Seattle WA 98101, USA.

[3] Department of Dermatology, University of California, San Francisco CA 94143, USA.

[4] Experimental & Clinical Cell Therapy Institute, Spinal Cord & Tissue Regeneration Center, Paracelsus Medical University, Salzburg, Austria.

[5] Department of Immunology, University of Washington School of Medicine, Seattle WA 98109, USA.

[6] EB House Austria, Department of Dermatology, University Hospital of the Paracelsus Medical University, Salzburg, Austria.

† First authors contributed equally

‡ Last authors contributed equally

*Corresponding authors: campbell@benaroyaresearch.org; iris.gratz@sbg.ac.at

One Sentence Summary: Functionally specialized human $CD4^+$ cutaneous resident memory T cells have the ability to exit the skin, are found in the circulation of healthy subjects, and can seed distant skin sites.

Abstract:

Tissue-resident memory T cells (T_{RM}) persist locally in non-lymphoid tissues, providing front-line defense against recurring insults. However, strict tissue compartmentalization of memory may pose certain disadvantages for a large barrier organ like the skin, and the long-term migratory behaviour of human T_{RM} and their contribution to the memory pool have not been fully elucidated. T_{RM} at barrier surfaces are defined in part by expression of the markers CD103 and/or CD69 which function to retain T_{RM} in epithelial tissues. Here, we found that $CD4^+CD69^+CD103^+$ T_{RM} in human skin can downregulate CD69, exit the tissue and be identified as a phenotypically unique population in the circulation of healthy individuals. These circulating T_{RM} produce the cytokines IL-22 and IL-13, and express genes consistent with a role in host-defense and tissue-repair responses. RNA- and TCR-sequencing demonstrated that $CD103^+$ T_{RM} in the blood are transcriptionally and clonally related to $CD69^+CD103^+$ T_{RM} in the skin. Furthermore, using a skin xenograft model, we confirmed that human cutaneous $CD103^+$ T_{RM} can exit the skin, enter the circulation, and recirculate to secondary human skin sites where they re-assume a T_{RM} phenotype. Thus, although as a population $CD4^+$ T_{RM} in the skin are largely sessile, recirculation of cutaneous $CD4^+CD103^+$ T_{RM} does occur in the steady state in humans, and these recirculating (rc)T_{RM} cells can promote the spread of this functionally specialized T cell population throughout the skin.

Introduction

T cell memory is compartmentalized into circulating and tissue-resident cell populations. Whereas circulating memory T cells continually patrol the body via the blood and lymphatics, tissue-resident memory T cells (T_{RM}) establish residence in non-lymphoid organs, where they can provide potent recall responses *(1)*. T_{RM} at barrier surfaces such as the intestines, lungs, and

skin are defined by expression of the markers CD103 and/or CD69, which together function to restrict their recirculation and maintain tissue residence *(2)(3)*. T_{RM} are thought to develop from effector or memory cells within the tissue itself, where they encounter tissue-derived signals that support their differentiation and maintenance *(4)*.

T_{RM} were first identified in the context of $CD8^+$ T cell responses to infection *(5)(6)*. Although cutaneous $CD8^+$ T_{RM} have been well-studied in the mouse, the behavior of $CD4^+$ memory T cells in mouse skin has been more controversial *(7)*. However, skin inflammation increased recruitment and retention of $CD4^+$ T cells in the skin *(8)(9)*, and cutaneous infection lead to the formation of sessile $CD69^+CD103^+$ $CD4^+$ T cells within the skin with superior effector functions *(10)(11)*. Still, in studying cutaneous $CD4^+$ T_{RM}, reliance on animal models can be problematic due to fundamental structural differences in the skin in humans versus mice, and a lack of direct correspondence between cutaneous T cell populations in these species. For instance, whereas nearly all $CD4^+$ T cells in murine skin are found in the dermis, the human epidermis is much thicker than in mice, and memory $CD4^+$ T cells can be found throughout human skin in both dermal and epidermal compartments *(2)*.

In human skin, most $CD4^+$ T cells express CD69, and studies following depletion of circulating T cells with anti-CD52 (alemtuzumab) indicated that these cells persist locally in the skin in the absence of continual replacement by circulating cells, defining them functionally as T_{RM} *(2)*. However, our understanding of how $CD4^+$ T_{RM} contribute to host-defense and pathogenic T cell responses in the skin is limited by the availability of appropriate clinical samples, and key questions regarding the origins, function and potential long-term migratory behavior of cutaneous $CD4^+$ T_{RM} in humans remain unanswered. Within the skin, T_{RM} are most abundant at the site of initial infection *(11)(12)*, and long-term maintenance of this

disequilibrium may pose a disadvantage for a large barrier organ like the skin where pathogen re-encounter at a secondary tissue site is possible. Therefore, we have analyzed the migratory behavior of cutaneous $CD4^+$ T_{RM}, taking advantage of new technological developments such as CyTOF, transcriptional profiling of small cell populations by RNA-sequencing, tissue explant cultures, and novel humanized mouse models we have developed.

We show $CD4^+CD69^+CD103^+$ T_{RM} in human skin can downregulate CD69, exit the tissue, and be identified as a distinct population in the blood of healthy donors. These circulating $CD4^+CD103^+$ cells share distinct phenotypic, functional and transcriptomic signatures with $CD103^+$ T_{RM} cells in the skin, and TCR repertoire analysis confirms the shared clonal origins of these populations. Using skin-humanized mice we further show that following exit from the skin, $CD4^+CD103^+$ memory cells can be recruited back into distant human skin sites and regain CD69 expression. Thus, although the majority of human cutaneous $CD4^+$ T_{RM} are tissue-resident in the skin, basal recirculation of these cells can be detected in the steady state, thereby promoting the spread of T_{RM} cells throughout this large barrier tissue.

Results

Cutaneous $CD4^+CD103^+$ T_{RM} cells can downregulate CD69 and exit the skin

Confirming prior analyses, we found that the vast majority of both $CD8^+$ and $CD4^+$ T cells in human skin expressed CD69, and a subset of $CD69^+$ cells also expressed the CD103 integrin and thus had the phenotype of alemtuzumab-resistant cutaneous T_{RM} *(2)* (Fig. 1, A and B; see Fig. S1 for representative T cell gating strategies from skin and blood). Consistent with their localization in the skin, most of these $CD69^+CD103^+$ T_{RM} also expressed the cutaneous lymphocyte antigen (CLA), a glycan moiety that promotes skin homing of immune cells by

acting as a ligand for E-selectin (Fig. 1C) *(13)*. To directly assess the ability of different skin T cell populations to exit the tissue, we performed tissue explant cultures using human skin obtained from surgical samples. Despite high expression of CD69 in the tissue, we found that a fraction of cutaneous $CD4^+CLA^+$ T cells exited the tissue in these explant cultures and could be detected in the culture media. This tissue exit was associated with downregulation of CD69 by a fraction of both $CD103^+$ and $CD103^-$ cells (Fig. 1, D and E). Importantly, healthy human skin contains virtually no $CD69^-CD103^+CD4^+$ T cells (Fig. 1, B and D), indicating that CD69 was indeed downregulated by $CD103^+$ T_{RM} in these cultures. Additionally, the $CD103^+$ cells that we detected in the media did not express the chemokine receptor CCR7, and thus these cells are distinct from $CD69^-CD103^{+/lo}$ cells that undergo CCR7-dependent migration from the skin to the draining lymph nodes in mice *(14)*, and from the $CCR7^+CD62L^-$ migratory memory (T_{MM}) cells described in human skin *(2)*. By contrast, very few $CD8^+$ T cells exited the skin in the explant cultures, consistent with more prolonged tissue-residency of this population in some mouse models *(15)*.

To determine if $CD4^+$ T_{RM} could exit the skin *in vivo*, we used a xenografting model in which human skin from a healthy donor was grafted onto immunodeficient NOD, scid, common-γ chain-deficient (NSG) mice *(16)*. T cells that had exited the skin were analyzed in the spleen. Similar to our explant studies, T cells exited the skin in all animals examined, including CLA^+CD103^+ T cells in 2 of the 3 recipient animals (Fig. 1, F and G). Importantly, expression of CD103 in the periphery is not induced by the xenogenic system we used, as we did not observe induction of CD103 expression by $CD4^+$ T cells in NSG mice upon transfer of total PBMC (Fig. S2).

Identification of T_{RM}-like cells in circulation of healthy humans

In addition to being found on T_{RM} in the skin, CLA is also present on a subset of circulating $CD45RA^{-}CD45RO^{+}$ memory T cells *(17)*. We noted that a fraction of those $CD4^{+}CLA^{+}$ memory T cells in human blood express CD103 (Fig. 1D) and therefore may represent T_{RM} that had exited from the skin and re-entered the circulation. To more comprehensively examine circulating $CLA^{+}CD103^{+}$ T cells and determine if they constitute a phenotypically distinct T cell subset, we first performed mass cytometry analysis of CLA^{+} T cells in the blood of 5 healthy subjects. Analysis by t-distributed Stochastic Neighbor Embedding (t-SNE) revealed 10 distinct clusters of $CD3^{+}CD45RA^{-}CLA^{+}$ memory T cells present in all subjects examined (Fig. 2A, Fig. S3), including 5 clusters of $CD4^{+}$ T cells (Fig. 2B). Interestingly, most $CD4^{+}CD103^{+}$ cells clustered together to form a discrete population (cluster 10) that was characterized by expression of CD103 and its dimerization partner β7 integrin. Cells in cluster 10 also expressed chemokine receptors strongly indicative of skin tropism such as CCR4, CCR6, and CCR10, but were largely negative for CCR7 (Fig. 2, B and C) *(18)(19)*. Additionally, cells in cluster 10 were low for expression of markers of regulatory T cells (Foxp3, CD25), T helper (Th)1 cells (CXCR3), Th17 cells (CD161) or natural killer T cells (CD56).

Using conventional flow cytometry, we further compared the abundance and phenotype of circulating $CD4^{+}CLA^{+}CD103^{+}$ to $CD4^{+}CLA^{+}CD103^{+}$ T_{RM} cells in the skin. In both blood and skin, CD103 and CCR7 clearly delineated 3 populations of CLA^{+} T cells (Fig. 3, A and B), but the distribution of these populations varied dramatically between sites. Whereas $CLA^{+}CD103^{+}$ memory T cells were common in the skin (26 +/- 9% of $CD4^{+}CLA^{+}$ T cells), they were a rare population in the blood, representing on average <2% of circulating $CLA^{+}CD45RA^{-}$ memory T cells, and <0.2% of total $CD4^{+}$ T cells (Fig. 3C, Fig. S4). By contrast, $CLA^{+}CCR7^{+}CD103^{-}$ were enriched in the blood relative to the skin, and the bulk of $CD4^{+}CLA^{+}$ T cells in both tissues were

CCR7$^-$CD103$^-$. CLA$^+$CD103$^+$ T$_{RM}$ in the skin shared the CCR4$^+$CCR6$^+$CXCR3$^-$ chemokine receptor profile with circulating CLA$^+$CD103$^+$ memory T cells, and CLA$^+$CD103$^+$ cells in the blood and all populations in the skin were mostly negative for CD49d (Fig. 3D). Like CD103, CD49d (also known as α4 integrin) can pair with β7 integrin, and in this combination promotes T cell localization to the intestinal mucosa (Fig. 3D) *(20)*. Similarly, like skin T$_{RM}$, most CLA$^+$CD103$^+$ cells in the blood were CD27$^-$ indicating that they are terminally differentiated *(21)*, whereas most circulating CLA$^+$CD103$^-$ memory T cells were CD27$^+$. Additionally, significant fractions of circulating CLA$^+$CD103$^+$ memory T cells expressed the markers CD101 and CD9, which were also expressed by the majority of CD103$^+$ T$_{RM}$ in the skin (Fig. 3E). Indeed, CD101 was recently identified as a marker of CD8$^+$CD103$^+$ T$_{RM}$ in various human tissues *(3)*, whereas CD9 is highly expressed by keratinocytes and T cells in the skin, where it modulates TGF-β signalling, integrin function, cell migration, and wound healing *(22)(23)*. However, consistent with downregulation of CD69 by T cells that migrated out of the skin in our tissue explant cultures, CLA$^+$CD103$^+$ cells in the blood were almost all CD69$^-$ (Fig. 3E).

CLA$^+$CD103$^+$ T cells from human blood and skin share a transcriptional and functional profile

To assess the transcriptional signature of circulating and skin-resident CLA$^+$CD103$^+$ T cells, we performed RNA-sequencing on sorted CLA$^+$ T cell populations from blood and skin (see Fig. S5 for sort scheme). Analysis of circulating CLA$^+$CD103$^+$ T cells identified a unique signature of 83 genes that were differentially expressed (false discovery rate (FDR) <0.05 and fold-change>2) compared to both CLA$^+$CD103$^-$CCR7$^-$ and CLA$^+$CD103$^-$CCR7$^+$ populations in the blood (Fig. 4A). The CD103$^+$ gene signature was also significantly enriched in CD103$^+$ vs. CD103$^-$ skin T$_{RM}$, consistent with the notion that circulating CLA$^+$CD103$^+$ cells represent mobilized CD103$^+$ T$_{RM}$ that downregulated CD69 to exit the skin (Fig. 4B). Indeed, hierarchical

clustering and principle component analysis (PCA) based on these genes clearly separated skin T_{RM} and circulating CLA^+CD103^+ cells from the two other populations of circulating CLA^+CD103^- memory T cells (Fig. 4, C and D). Finally, we used the $CD103^+$ gene signature to perform PCA on publicly available transcriptional profiles of $CD69^+$ and $CD69^-$ $CD4^+$ T cells isolated from human lung and spleen *(3)*. This gene signature, derived solely from circulating CLA^+CD103^+ T cells, clearly distinguished $CD69^+$ T_{RM} from $CD69^-$ cells in both organs (Fig. 4E), and this further supports the transcriptional link between CLA^+CD103^+ cells in the blood and T_{RM} in multiple tissue sites.

CD103 expression by T_{RM} is induced upon migration into non-lymphoid sites by tissue-derived factors including TGF-β *(4)*. Consistent with this, several TGF-β related genes are upregulated in circulating and skin-resident CLA^+CD103^+ cells (Fig. 4F and Fig. S6). Moreover, along with *ITGAE* (the gene encoding CD103)*, CD27* and *CD101*, we found several additional T_{RM}-associated genes differentially expressed by circulating CLA^+CD103^+ cells, including *CCR8 (24), CXCR6 (3), EOMES (25) and PPARG (26)*. We also identified overlapping functional modules of genes differentially expressed by CLA^+CD103^+ T cells that control cellular migration and adhesion, and that modulate host defense and tissue inflammation (Fig. 4F and Fig. S6).

To complement this transcriptomic study, we assessed the function of memory T cells from skin and blood following *ex vivo* stimulation and intracellular cytokine staining. Among effector cytokines, production of IL-22 and IL-13 was significantly enriched in CLA^+CD103^+ cells from both organs, but these cells were largely negative for IFN-γ, IL-17A or IL-4 (Fig. 5). Although GM-CSF production was also highly enriched in CLA^+CD103^+ cells in the blood, production in the skin was low in all T cell populations (Fig. 5, D and E). This cytokine

phenotype is consistent with that of Th22 cells *(27)(28)*, and distinguished CLA^+CD103^+ T cells from CLA^+CD103^- and CLA^-CD103^- T cells in both skin and blood. Co-production of IL-22 and IL-13 (Fig. S7) is indicative of a role for CLA^+CD103^+ T cells in promoting normal tissue homeostasis and repair in the skin *(29)(30)*. Accordingly, CLA^+CD103^+ cells in the blood and skin differentially expressed a set of genes implicated in tissue-repair responses, as well as the receptor components for the epithelial-derived cytokine IL-25 (*IL17RA, IL17RB)* (Fig. 4F, Fig. S6). This suggests that CLA^+CD103^+ cells have the ability to directly sense IL-25 produced by keratinocytes upon tissue damage or cellular stress *(31)*.

CLA^+CD103^+ T cells from human blood and skin are clonally related

Their shared phenotype, function and transcriptomic signature suggests that CLA^+CD103^+ T cells in blood and skin are closely related. To directly determine if CLA^+CD103^+ T cells in skin and blood have a shared clonal origin, we performed TCRβ sequencing on 5 populations of CLA^+ T cells sorted based on differential expression of CD103 and CCR7 from paired blood and skin samples from four individual donors as in Fig. 4. Analysis of unique CDR3 clonotypes showed that sequences from CLA^+CD103^+ T_{RM} cells from the skin were also found at high frequency in the circulating CLA^+CD103^+ cells. Clonotypes of skin CLA^+CD103^+ T cells were also found in CLA^+CD103^- T cells from the skin, whereas little clonal overlap was observed with circulating $CLA^+CD103^-CCR7^+$ and $CLA^+CD103^-CCR7^-$ T cells (Fig. 6A, left and Fig. S8A). Quantitative analysis of TCR repertoire overlap using the Morisita index, which accounts for both species presence and abundance, confirmed that the repertoire of CLA^+CD103^+ T cells in skin is most similar to the circulating CLA^+CD103^+ T cells (Fig 6A, right). Reciprocally, circulating CLA^+CD103^+ cells from the blood showed the highest TCR repertoire overlap with skin CLA^+CD103^+ T cells (Fig 6B, Fig. S8A). Taken together, these

analyses demonstrate the shared clonal origin of the CLA^+CD103^+ T cell populations in the blood and skin, thereby providing strong evidence that the CLA^+CD103^+ T cells in the blood represent the circulating counterparts of cutaneous CLA^+CD103^+ T_{RM}. Notably, CLA^+CD103^+ T cells in both blood and skin showed diverse Vβ usage (Fig. S8B), and there was no overlap in the TCRβ sequences in any of the populations examined between the 4 different donors. Thus, CLA^+CD103^+ T cells in the blood and skin do not appear to be a clonally restricted or invariant T cell population such as NK T cells or mucosa-associated invariant T (MAIT) cells.

Circulating CLA^+CD103^+ T_{RM} can reseed distant skin sites

Exit of cutaneous $CD4^+CD103^+$ T_{RM} may allow these cells to migrate to distant tissue sites and promote the efficient distribution of these functionally specialized cells throughout the skin. To directly test this hypothesis *in vivo*, we employed a mouse xenografting model designed to track tissue exit of human cutaneous T_{RM} and their subsequent migration to secondary human skin sites. This was accomplished by generating engineered skin (ES) from cultured human keratinocytes and fibroblasts. In this system, cell suspensions of keratinocytes and fibroblasts are placed in a grafting chamber that is surgically implanted on NSG mice. The cells undergo spontaneous cell sorting to form epidermal and dermal layers, generating skin tissue with histological features of human skin as well as the organotypic expression of structural proteins such as human type VII collagen at the epidermal-dermal junction (Fig. 7A) *(32)*. Thus, the ES closely resembles human skin but lacks resident immune cells, and therefore T cell migration into the ES can be definitively monitored. After healing of the ES (>110 days), mice received skin grafts from healthy donors, and tissues were analyzed three to five weeks later (Fig. 7, B and C). $CD4^+CLA^+$ T cells had exited the skin grafts and were found in both the spleens (in all recipients; as in Fig. 1, F and G) and ES (in 6 of 7 recipients). Moreover, a portion of the cells

found in the ES were CLA^+CD103^+ (Fig. 7, D and E), whereas no human cells were found in adjacent murine skin (Fig. S9). Similar to what we observed in human blood and skin, CD9 and CD69 were downmodulated on CLA^+CD103^+ T cells that exited the skin and were found in the spleen, but re-expressed by cells entering the ES, whereas CD27 expression was low in all tissue sites (Fig. 7F). Finally, we used this system to interrogate the *in vivo* migration behaviour of circulating CLA^+CD103^+ T cells from the blood of a healthy human donor. Upon PBMC transfer into NSG mice carrying ES (Fig. 7G), we found that T cells migrated to the ES, and that CLA^+CD103^+ cells were significantly enriched in the ES versus the spleen (Fig. 7, H and I). Together, these data demonstrate that T_{RM} that exit from the skin upon grafting or are found in the blood of healthy individuals have the ability to migrate to and populate secondary skin sites.

Discussion

T_{RM} have been defined as non-circulating cells that mediate optimal protective responses to site-specific challenges through rapid activation of an immune response *in situ (33)(2)*. However, using tissue explant cultures and a novel skin-humanized mouse model designed to directly examine the migratory behavior of human T_{RM}, we found that $CD4^+CD69^+CD103^+$ T_{RM} in human skin can downregulate CD69 and exit the tissue. This is consistent with recent observations in murine systems showing that secondary stimulation could mobilize $CD8^+$ T cells from non-lymphoid tissues (including the skin) that subsequently established residence within draining secondary lymphoid organs (SLO) *(34)*. However, this study did not establish from which population of skin-resident cells these SLO T_{RM} were derived, or whether these mobilized cells recirculated to other peripheral non-lymphoid tissue sites. We have now identified $CD4^+CLA^+CD103^+$ as a distinct population of circulating T cells that are clonally related to and

share phenotypic, functional and transcriptomic signatures with $CD4^+CD103^+$ T_{RM} in the skin. We also show that upon exiting the skin, $CLA^+CD103^+CD69^-$ cells can migrate via the circulation to secondary skin sites where they re-acquire markers of tissue residence such as CD69. Based on these features, we propose that these cells are the recirculating counterparts of cutaneous $CD103^+$ T_{RM}, or rcT_{RM} cells.

In addition to their phenotypic similarity, we defined a transcriptional signature of human cutaneous $CD103^+$ T_{RM} cells based solely on analysis of $CD103^+$ rcT_{RM} isolated from the circulating pool of CLA^+ skin-tropic T cells. Interestingly, our analysis also indicates that this set of signature genes shared by rcT_{RM} and skin T_{RM} may be suitable to identify T_{RM} in multiple human tissues, and this therefore extends recent studies in which the phenotypic and transcriptional signatures of pulmonary and splenic T_{RM} were defined *(3)*. However, whether in-depth analysis of additional memory populations with distinct tissue-tropism will reveal rcT_{RM} from other large barrier tissues, particularly the gut, remains to be determined.

The transcriptional signature of $CD103^+$ rcT_{RM} revealed several unique and interesting features shared by CLA^+CD103^+ cells in blood and skin. For instance, these populations shared expression of several TGF-β associated genes, consistent with the proposed role for this cytokine in the upregulation of CD103 and development of skin T_{RM} *(4)(35)*. The transcriptional and functional profile of $CD103^+$ T_{RM} and rcT_{RM} is also indicative of a function in normal wound-healing and tissue-repair responses. Human skin-resident αβ T cells can promote tissue-repair in skin organ culture models *(36)*, but further phenotypic and functional characterization of skin T cells capable of accelerating wound healing has not been performed. The signature cytokines produced by CLA^+CD103^+ T cells, IL-22 and IL-13, both have important tissue-repair function in the skin. IL-22 acts directly on keratinocytes to promote their survival, proliferation, migration

and anti-microbial functions *(30)*, whereas IL-13 activates cutaneous fibroblasts and promotes M2 macrophage differentiation and wound healing *(37)*. RNA sequencing further identified a set of signature genes shared by $CD103^+$ T_{RM} cells in blood and skin consistent with a role in promoting tissue-repair responses and barrier function, including *CD9 (23), MUC16 (38)(39),* and *LGALS3 (40)*. Moreover, CLA^+CD103^+ cells in both skin and blood express receptors for the epithelial-derived cytokine IL-25, which can potentiate IL-13 production by multiple cell types and thereby accelerate tissue repair responses and contribute to development of fibrosis *(29)*. Thus, although the precise role of these cells in skin immunity and homeostasis remains to be established, the phenotypic, functional and transcriptional profile of circulating CLA^+CD103^+ rcT_{RM} cells is consistent with their origin and function within the skin, a TGF-β-rich barrier site exposed to microbial threats and frequent tissue damage.

Mobilization of T_{RM} from the skin to seed distant sites appears to contradict the idea that T_{RM} are retained locally in the tissue long-term. However, our data are consistent with a model where T_{RM} transiently forgo their tissue-location to re-assume residency at distant sites of the tissue. Additionally, it is important to note that when we combine the frequency of circulating $CD103^+$ rcT_{RM} and skin T_{RM} with estimates of T cell numbers in human skin and blood *(13)*, rcT_{RM} make up less than 1% of all CLA^+CD103^+ memory cells in the body at any given time (Table S1). Whether exit of $CD103^+$ T_{RM} cells is a stochastic process or actively triggered mobilization remains to be determined. In the context of our studies in explant cultures and in skin-humanized mice, tissue damage unavoidably associated with surgical skin acquisition is one potential trigger that may have impacted T_{RM} mobilization. However, we detected CLA^+CD103^+ rcT_{RM} in the blood of all healthy donors analyzed, which indicates that a small fraction of T_{RM}

continually exits the skin even in the absence of clinical skin infection, inflammation or tissue damage.

Our xenografting studies were designed to further follow the fate of rcT$_{RM}$, and we found that CD103$^+$ rcT$_{RM}$ from either skin grafts or from human blood can migrate to and seed secondary skin sites. This tissue-seeding occurred in the absence of tissue damage or local inflammation since the recipient skin tissue (i.e. engineered skin devoid of T$_{RM}$) was fully healed (>110 days) and thus likely lacked expression of damage-associated molecules that might increase recruitment of rcT$_{RM}$. However, it remains possible that recruitment to secondary skin sites is increased by damage-associated stress. This might offer an intriguing explanation to the hitherto unexplained Koebner phenomenon (KP), in which lesions in T$_{RM}$-mediated diseases such as psoriasis and mycosis fungoides spread to otherwise healthy (non-infected) skin sites upon triggers such as mechanical trauma, burns, friction or UV-irradiation *(41)(42)(43)*.

Collectively, our data reveal the migratory behaviour of CD4$^+$ T$_{RM}$ from healthy human skin, thereby challenging current concepts regarding the strict tissue compartmentalization of T cell memory in humans. Mobilization of a fraction of CD4$^+$ T$_{RM}$ to the circulation might support the distribution of immunity in a large barrier organ such as the skin, as well as provide a reservoir of circulating T cells that could be rapidly recruited to infected or damaged skin to promote host-defense and tissue-repair. Importantly, our identification of rcT$_{RM}$ as a unique population of circulating CLA$^+$ T cells in healthy subjects greatly facilitates the isolation and study of T$_{RM}$-like cells from a broadly available human tissue, the blood. This promises to yield new insights into the biology and function of human skin T$_{RM}$ cells, and opens novel avenues to therapeutically manipulating T$_{RM}$ in the context of T$_{RM}$-associated diseases such as psoriasis or mycosis fungoides, where limiting the spread of pathogenic cells is desirable*(44)*.

Material and Methods

Study design. The objective of this research was to characterize the phenotype, function and migratory behaviour of $CD4^+$ T cell populations that express the cutaneous lymphocyte antigen (CLA), and to define the relationship between CLA^+ T cells in the blood and CLA^+ T_{RM} cells in the skin. This was accomplished using blood and skin samples from healthy donors by flow cytometric analysis of cellular phenotype and function, transcriptomic analysis by RNA-sequencing, T cell receptor clonotype analysis by TCR-sequencing, and experimental studies of cellular behaviour in explant culture models and skin xenograft studies using immunodeficient mice. Blood samples from healthy donors was obtained by standard phlebotomy. Normal human skin was obtained from patients undergoing elective surgery (panniculectomy, elective breast reduction), in which skin was discarded as a routine procedure. In one case, skin and blood was obtained from a treatment naïve subject undergoing surgery for mammary carcinoma, and data from this subject is specifically marked in the figures. Samples of subjects of both sexes were included in the study. Ages ranged from 17 - 70. All samples were obtained upon written informed consent at the University Hospital Salzburg, Austria, or the Virginia Mason Medical Center in Seattle, WA, USA. All studies were approved by the Salzburg state Ethics Commission (decision: according to Salzburg state hospital law no approval required) (Salzburg, Austria) or the Institutional Review Board of the Benaroya Research Institute (Seattle, WA). NOD.Cg-Prkdcscid Il2rgtm1Wjl/SzJ (NSG) mice were obtained from The Jackson Laboratory and bred and maintained in a specific pathogen-free facility in accordance with the guidelines of the Central Animal Facility of the University of Salzburg. All animal studies were approved by the Austrian Federal Ministry of Science, Research and Economy. No statistical method was used to

predetermine sample size. Samples sizes were based on the availability of human blood and skin specimens and were large enough to ensure achieve a greater than 80% probability of identifying an effect of >20% in measured variables. 2-3 independent experiments (biological replicates) were conducted to validate each finding. In RNA sequencing, samples were excluded from the analysis based on pre-established quality control criteria: Samples with a total number of fastq reads $<1x10^6$, mapped reads below 70% or median CV coverage >1 were excluded from further analysis. Randomization was not applicable because no treatment or intervention groups were included in the study. Blinding was not applicable since no treatment groups were compared.

Skin explant cultures. Skin was washed in PBS with 1% Pen/Strep and 0.1% Primocin (Invivogen; ant-pm-1) for 5 minutes. Small skin pieces of 1-2mm were generated using forceps and sharp scissors. Pieces were placed in 60mm dish and allowed to adhere for 10 minutes. Crawl-out medium consisting of 50% Epilife (Gibco, MEPICF500) and 50% RPMI-complete (RPMIc: RPMI 1640 (Gibco; 31870074) with 5% human serum (Sigma-Aldrich; H5667 or H4522), 1% penicillin/streptomycin (Sigma-Aldrich; P0781), 1% L-Glutamine (Gibco; A2916801), 1% NEAA (Gibco; 11140035), 1% Sodium-Pyruvate (Sigma-Aldrich; S8636) and 0.1% β-Mercaptoethanol (Gibco; 31350-010)) was added to explant cultures. Seven days later, cells in culture medium were analyzed by flow cytometry.

Cytometry by time-of-flight (CyTOF). Human frozen PBMCs were thawed and rested for 12-15h. The samples were washed with Ca- and Mg-free PBS (Sigma; D8537) and stained with 50μM Cisplatin (Enzo Life Sciences; ALX-400-040-M250) in PBS for 1 minute to exclude dead cells. The cells were washed and resuspended with Human TruStain FcX (Biolegend; 422302) for five minutes before adding the primary surface staining cocktail for 20m, washing and

staining with the secondary surface cocktail for 20m. Intracellular staining was performed following fixation and permeabilization using the Maxpar Nuclear Antigen Staining Buffer Set (Fluidigm; 201063) for 60 minutes, after which cells were incubated overnight at 4°C with Maxpar Fix and Perm Solution containing 125nM Cell-ID Intercalator-Ir (Fluidigm; 201192A) for DNA staining. Cells were washed with MilliQ H_2O and resuspended in MilliQ H_2O spiked with 1/20th Maxpar EQ Four Element Calibration Beads (Fluidigm; 201078) to a density of <500.000 cells/mL. Data was acquired on a CyTOF 1.5 (Fluidigm) instrument. For analysis, FCS files on gated $CD3^+CLA^+$ cells were generated using FlowJo software (Tree Star, Inc.). t-distributed Stochastic Neighbor Embedding (t-SNE) analysis was performed in R using the cytofkit R package, and clustering was performed with FlowSOM.

T cell isolation from skin for flow cytometry and RNAseq. Tissues were minced and digested using collagenase type 4 and DNase as previously described *(45)*. Briefly, subcutaneous fat was removed before skin was minced with dissection scissors and surgical scalpel. Approximately $1cm^2$ of skin was digested overnight in 5%CO_2 at 37°C with 3ml of digestion mix containing 0.8mg/ml Collagenase Type 4 (Worthington; #LS004186) and 0.02mg/ml DNase (Sigma-Aldrich; DN25) in RPMIc. Samples were filtered, washed with RPMI and PBS and stained for flow cytometry/cell sorting or stimulated for intracellular cytokine staining.

PBMC isolation for flow cytometry and RNAseq. Human PBMCs were isolated using Ficoll-Hypaque (GE-Healthcare; GE17-1440-02) gradient separation. For RNAseq $CD4^+$ T cells were enriched using CD4 microbeads (Miltenyi; 130-045-101) and $4x10^6$ cells/ml were resuspended in RPMIc with 50 U/ml IL-2 (Immunotools; 11340023) in a 24-well and stimulated for 20h with

25µl/ml ImmunoCult CD3/CD28 T cell activator (Stemcell; 10971) prior to staining and cell sorting.

Flow cytometry. For sorting, cells were stained in FACS buffer (PBS + 1 % FBS +1 mM EDTA) for surface markers. For detection of intracellular cytokine production, skin single cell suspensions and PBMCs were stimulated with 50 ng/ml PMA (Sigma-Aldrich; P8139) and 1 µg/ml Ionomycin (Sigma-Aldrich; I06434) with 10 µg/ml Brefeldin A (Sigma-Aldrich; B6542) for 3.5 hrs. For permeabilization and fixation Cytofix/Cytoperm kit was used (BectonDickinson; RUO 554714). Data were acquired on LSR Fortessa, LSRII (both BD Biosciences) or Cytoflex LS (Beckman Coulter) flow cytometers and analyzed using FlowJo software (Tree Star, Inc.)

RNA sequencing. 500 cells per population were sorted into lysis buffer using a BD FACSARIA III or FACSFUSION instruments (BD Biosciences), and cDNA was prepared using the SMART-Seq v4 Ultra Low Input RNA Kit for Sequencing (Takara). Library construction was performed using the NexteraXT DNA sample preparation kit (Illumina) using half the recommended volumes and reagents. Dual-index, single-read sequencing of pooled libraries was run on a HiSeq2500 sequencer (Illumina) with 58-base reads and a target depth of 5 million reads per sample. Base-calling and demultiplexing were performed automatically on BaseSpace (Illumina) to generate FASTQ files.

RNAseq analysis. The FASTQ files were processed in order to remove reads of zero length (fastq_trimmer v.1.0.0), remove adapter sequences (fastqmcf tool v.1.1.2) and perform quality trimming from both ends until a minimum base quality ≥ 30 (FASTQ quality trimmer tool v.1.0.0). Reads were aligned to the human reference genome (build hg38) with TopHat (v.1.4.0) and read counts per Ensembl gene ID were quantified with htseq-count (v.0.4.1). Quality metrics

for the FASTQ and BAM/SAM files were generated with FastQC (v.0.11.3) and Picard (v.1.128). Processing of FASTQ and BAM/SAM files was executed on the Galaxy workflow platform of Globus genomics. Statistical analysis of gene expression was assessed in the R environment (v.3.4.4). Samples with a total number of fastq reads below 10^6, mapped reads below 70% or median CV coverage > 1 were excluded from further analysis. Mapping Ensembl Gene IDs to HGNC gene symbols was achieved through biomaRt (GRCh38.p10). Genes were filtered for protein coding genes and those with an expression of CPM > 2 in at least 10% of the libraries. A linear model for gene expression was fit to the filtered 12,293 genes using limma (v3.34.9)*(46)*, considering donor effects through a random factor. For visualizations the random effect of the model was approximated by removing the donor effect from the expression data with limma::removeBatchEffect. Genes found to be significantly different (adj.p.val < 0.05 and fold-change>2) between $CD103^+$ cells and $CD103^-CCR7^+$ cells as well as between $CD103^+$ cells and $CD103^-CCR7^-$ cells in the blood were defined as the $CD103^+$ gene signature. Enrichment of the $CD103^+$ gene signature in the ranked list of $CD103^+$ cells vs $CD103^-CCR7^-$ cells in the skin was visualized with limma::barcodeplot and significance determined by rotation gene set testing with limma::roast. Publicly available data on human $CD4^+$ Tissue-Resident Memory T Cells was retrieved from GEO dataset GSE94964. Gene names were lifted over from hg19 to hg38 nomenclature, the limma::voom transformed expression values were corrected for donor effect with sva::ComBat and PCA was performed on genes from the $CD103^+$ signature or the same number of randomly selected genes.

TCRβ sequencing and analysis. A minimum of 2,000 cells T cells from the indicated populations were sorted into RPMIc, and genomic DNA was prepared using the QIAamp DNA Micro Kit (Qiagen). Amplification and sequencing was performed using the immunoSEQ®

Assay (Adaptive Biotechnologies, Seattle, WA), which combines multiplex PCR with high throughput sequencing and a bioinformatics pipeline for TCRβ CDR3 analysis *(47)*. Data analysis was performed using Adaptive Biotechnologies ImmunoSeq Analyzer 3.0 software and R version 3.5.1. Data for the analysis in R was exported through the export function in the Rearrangement details view. Circle plots for individual donors were created by downsampling populations with more than 1000 unique rearrangements (weighted based on relative abundance of each individual clonotype) and matching TCR chains with the R package TCRtools (https://github.com/mjdufort/TCRtools). Links between the blood or skin $CD103^+$ reference population and all other populations are displayed in the circle plot. For V gene usage, we removed unknown and ambiguous mappings and computed the percentage of clones using each V gene among each sample. The plot includes V genes that have a usage ≥ 5% in at least one sample.

Generation of engineered skin (ES). Human keratinocytes and fibroblasts were isolated from normal human skin and immortalized using human papilloma viral oncogenes E6/E7 HPV as previously described *(48)*. These were cultured in Epilife (Gibco, MEPICF500) and DMEM (Gibco; 11960-044) containing 2% L-Glutamine, 1% Pen/Strep, 10% FBS, respectively. For transplantation, 80% confluent cells were trypsinized (TrypLE express, Gibco; 12604021) washed with PBS and counted. Per mouse, $1\text{-}2x10^6$ keratinocytes were mixed 1:1 with autologous fibroblasts in 400µl MEM(Gibco; 11380037) containing 1% FBS, 1% L-Glutamine and 1% NEAA were used for *in vivo* generation of engineered skin as described *(32)*.

Transplantation of human skin or PBMC transfer. 8mm punch biopsies of human skin were trimmed to an average thickness of 0.5-1mm. Transplants were soaked in PBS + 1% Pen/Strep +

0.1% Primocin (Invitrogen; ant-pm-1) for 5 minutes and kept on ice in a sterile container with PBS soaked gauze until transplantation. NSG mice were anesthetized and full thickness wound bed prepared using surgical scissors. Three grafts/mouse were placed on the back and fixed using surgical skin glue (Histoacryl; BRAUN). Transplants were covered with paraffin gauze dressing and bandaged with self-adhesive wound dressing. Bandages were removed after 7 days. In other experiments PBMC were thawed and rested in media over night before transfer into NSG recipient mice ($2.5x10^6$ cells/animal). After transfer of human cells (PBMC or skin grafting) mouse neutrophils were depleted with anti-Gr-1 antibody (InVivoMab clone RB6-8C5; 100 µg Gr-1-Ab/animal i.p. every 5-7 days) *(49)(50)*.

Histological staining of skin sections. Normal human skin, engineered skin grafts and adjacent murine skin was excised and frozen in TissueTek O.C.T. Compound (Sakura; TTEK). 7 µm cryosections were stained with Hemalum solution acid (Carl Rorth; T865.1) and Eosin Y aqueous solution (Sigma, 201192A). Human type VII collagen was stained by immunofluorescence using anti-human type VII collagen antibody (anti-NC-1 domain of type VII collagen (LH7.2) kindly provided by Dr. Alexander Nyström, University of Freiburg, Germany) and goat anti-rabbit A488 (ThermoFisher; A11008) secondary antibody, and nuclear DAPI staining (ProLong™ Gold Antifade Mountant with DAPI, Invitrogen; P36931).

Tissue preparation from mice. Mice were euthanized using CO_2 asphyxiation followed by cervical dislocation. Single cell suspensions were generated from spleen, engineered skin and human skin grafts and leukocytes analyzed by flow cytometry.

Statistical analysis. Statistical significance of data was calculated with Prism 6.0 software (GraphPad) by one-way ANOVA with Tukey's or Dunnett's multiple comparisons test, or by paired t-test as indicated. Error bars indicate mean + standard deviation.

Detailed list of antibodies and reagents can be found in supplementary Table S2

Supplementary Materials

Supplementary Data Methods

T cell isolation from murine skin for flow cytometry. Approx. 3 cm^2 of shaved dorsal mouse skin were harvested and single cell suspensions prepared as in *(51)* and stained for flow cytometry.

List of Supplementary Figures

Fig. S1: Representative flow cytometry gating strategies used to identify T cell subsets in human blood and skin.

Fig. S2: CD103 expression is not induced on human $CD4^+$ T cells in NSG mice.

Fig. S3: CyTOF analysis of CLA^+ T cells in PBMC.

Fig. S4: Frequencies of CLA^+ T cell subsets in blood and skin.

Fig. S5: Experimental schematic of cell isolation and sort gates for RNA-seq.

Fig. S6: Graphical analyses showing expression of the indicated genes in the different populations of $CD4^+CLA^+$ T cells from blood and skin as determined by RNA-seq.

Fig. S7: $CD103^+CLA^+$ T cells from human blood and skin coproduce IL-22 and IL-13.

Fig. S8: Analysis of TCRβ repertoire overlap and Vβ gene usage in CLA^+ T cells from blood and skin.

Fig. S9: Human skin-derived cells do not infiltrate murine skin.

Table S1: CLA^+CD103^+ T cells in circulation constitute a minor fraction of all CLA^+CD103^+ T cells.

Table S2: Detailed list of antibodies and reagents

References

1. S. N. Mueller, L. K. Mackay, Tissue-resident memory T cells: local specialists in immune defence, *Nat. Rev. Immunol.* **16**, 79–89 (2016).

2. R. Watanabe, A. Gehad, C. Yang, L. Campbell, J. E. Teague, C. Schlapbach, C. Elco, V. Huang, T. R. Matos, T. S. Kupper, R. A. Clark, Human skin is protected by four functionally and phenotypically discrete populations of resident and recirculating memory T cells, *Sci Transl Med* **7**, 279ra39 (2015).

3. B. V. Kumar, W. Ma, M. Miron, T. Granot, R. S. Guyer, D. J. Carpenter, T. Senda, X. Sun, S.-H. Ho, H. Lerner, A. L. Friedman, Y. Shen, D. L. Farber, Human tissue-resident memory T cells are defined by core transcriptional and functional signatures in lymphoid and mucosal sites, *Cell Rep* **20**, 2921–2934 (2017).

4. L. K. Mackay, A. Rahimpour, J. Z. Ma, N. Collins, A. T. Stock, M.-L. Hafon, J. Vega-Ramos, P. Lauzurica, S. N. Mueller, T. Stefanovic, D. C. Tscharke, W. R. Heath, M. Inouye, F. R. Carbone, T. Gebhardt, The developmental pathway for CD103(+)CD8+ tissue-resident memory T cells of skin, *Nat. Immunol.* **14**, 1294–1301 (2013).

5. K. D. Klonowski, K. J. Williams, A. L. Marzo, D. A. Blair, E. G. Lingenheld, L. Lefrançois, Dynamics of blood-borne CD8 memory T cell migration in vivo, *Immunity* **20**, 551–562 (2004).

6. T. Gebhardt, L. M. Wakim, L. Eidsmo, P. C. Reading, W. R. Heath, F. R. Carbone, Memory T cells in nonlymphoid tissue that provide enhanced local immunity during infection with herpes simplex virus, *Nat. Immunol.* **10**, 524–530 (2009).

7. T. Gebhardt, P. G. Whitney, A. Zaid, L. K. Mackay, A. G. Brooks, W. R. Heath, F. R. Carbone, S. N. Mueller, Different patterns of peripheral migration by memory CD4+ and CD8+ T cells, *Nature* **477**, 216–219 (2011).

8. N. Collins, X. Jiang, A. Zaid, B. L. Macleod, J. Li, C. O. Park, A. Haque, S. Bedoui, W. R. Heath, S. N. Mueller, T. S. Kupper, T. Gebhardt, F. R. Carbone, Skin CD4+ memory T cells exhibit combined cluster-mediated retention and equilibration with the circulation, *Nature Communications* **7**, 11514 (2016).

9. L. K. Beura, S. E. Hamilton, K. Bi, J. M. Schenkel, O. A. Odumade, K. A. Casey, E. A. Thompson, K. A. Fraser, P. C. Rosato, A. Filali-Mouhim, R. P. Sekaly, M. K. Jenkins, V. Vezys, W. N. Haining, S. C. Jameson, D. Masopust, Normalizing the environment recapitulates adult human immune traits in laboratory mice, *Nature* **532**, 512–516 (2016).

10. N. D. Glennie, V. A. Yeramilli, D. P. Beiting, S. W. Volk, C. T. Weaver, P. Scott, Skin-resident memory CD4+ T cells enhance protection against Leishmania major infection, *J. Exp. Med.* **212**, 1405–1414 (2015).

11. C. O. Park, X. Fu, X. Jiang, Y. Pan, J. E. Teague, N. Collins, T. Tian, J. T. O'Malley, R. O. Emerson, J. H. Kim, Y. Jung, R. Watanabe, R. C. Fuhlbrigge, F. R. Carbone, T. Gebhardt, R. A. Clark, C. P. Lin, T. S. Kupper, Staged development of long-lived T-cell receptor αβ TH17 resident memory T-cell population to Candida albicans after skin infection, *J. Allergy Clin. Immunol.* **142**, 647–662 (2018).

12. B. Davies, J. E. Prier, C. M. Jones, T. Gebhardt, F. R. Carbone, L. K. Mackay, Cutting Edge: Tissue-Resident Memory T Cells Generated by Multiple Immunizations or Localized Deposition Provide Enhanced Immunity, *J. Immunol.* **198**, 2233–2237 (2017).

13. R. A. Clark, B. Chong, N. Mirchandani, N. K. Brinster, K.-I. Yamanaka, R. K. Dowgiert, T. S. Kupper, The vast majority of CLA+ T cells are resident in normal skin, *J. Immunol.* **176**, 4431–4439 (2006).

14. S. K. Bromley, S. Yan, M. Tomura, O. Kanagawa, A. D. Luster, Recirculating memory T

cells are a unique subset of CD4+ T cells with a distinct phenotype and migratory pattern, *J. Immunol.* **190**, 970–976 (2013).

15. T. Gebhardt, L. K. Mackay, Local immunity by tissue-resident CD8(+) memory T cells, *Front Immunol* **3**, 340 (2012).

16. M. King, T. Pearson, L. D. Shultz, J. Leif, R. Bottino, M. Trucco, M. A. Atkinson, C. Wasserfall, K. C. Herold, R. T. Woodland, M. R. Schmidt, B. A. Woda, M. J. Thompson, A. A. Rossini, D. L. Greiner, A new Hu-PBL model for the study of human islet alloreactivity based on NOD-scid mice bearing a targeted mutation in the IL-2 receptor gamma chain gene, *Clin. Immunol.* **126**, 303–314 (2008).

17. R. C. Fuhlbrigge, J. D. Kieffer, D. Armerding, T. S. Kupper, Cutaneous lymphocyte antigen is a specialized form of PSGL-1 expressed on skin-homing T cells, *Nature* **389**, 978–981 (1997).

18. M. M. Klicznik, A. B. Szenes-Nagy, D. J. Campbell, I. K. Gratz, Taking the lead - how keratinocytes orchestrate skin T cell immunity, *Immunol. Lett.* **200**, 43–51 (2018).

19. T. S. Kupper, R. C. Fuhlbrigge, Immune surveillance in the skin: mechanisms and clinical consequences, *Nat. Rev. Immunol.* **4**, 211–222 (2004).

20. C. Berlin, E. L. Berg, M. J. Briskin, D. P. Andrew, P. J. Kilshaw, B. Holzmann, I. L. Weissman, A. Hamann, E. C. Butcher, Alpha 4 beta 7 integrin mediates lymphocyte binding to the mucosal vascular addressin MAdCAM-1, *Cell* **74**, 185–195 (1993).

21. R. D. Fritsch, X. Shen, G. P. Sims, K. S. Hathcock, R. J. Hodes, P. E. Lipsky, Stepwise differentiation of CD4 memory T cells defined by expression of CCR7 and CD27, *J. Immunol.* **175**, 6489–6497 (2005).

22. R. Reyes, B. Cardeñes, Y. Machado-Pineda, C. Cabañas, Tetraspanin CD9: A Key Regulator of Cell Adhesion in the Immune System, *Front Immunol* **9**, 863 (2018).

23. J. Zhang, J. Dong, H. Gu, S. Yu, X. Zhang, Y. Gou, W. Xu, A. Burd, L. Huang, K. Miyado, Y. Huang, H. C. Chan, CD9 is critical for cutaneous wound healing through JNK signaling, *J. Invest. Dermatol.* **132**, 226–236 (2012).

24. M. L. McCully, K. Ladell, R. Andrews, R. E. Jones, K. L. Miners, L. Roger, D. M. Baird, M. J. Cameron, Z. M. Jessop, I. S. Whitaker, E. L. Davies, D. A. Price, B. Moser, CCR8 Expression Defines Tissue-Resident Memory T Cells in Human Skin, *J. Immunol.* **200**, 1639–1650 (2018).

25. L. K. Mackay, E. Wynne-Jones, D. Freestone, D. G. Pellicci, L. A. Mielke, D. M. Newman, A. Braun, F. Masson, A. Kallies, G. T. Belz, F. R. Carbone, T-box Transcription Factors Combine with the Cytokines TGF-β and IL-15 to Control Tissue-Resident Memory T Cell Fate, *Immunity* **43**, 1101–1111 (2015).

26. Y. Pan, T. Tian, C. O. Park, S. Y. Lofftus, S. Mei, X. Liu, C. Luo, J. T. O'Malley, A. Gehad, J. E. Teague, S. J. Divito, R. Fuhlbrigge, P. Puigserver, J. G. Krueger, G. S. Hotamisligil, R. A. Clark, T. S. Kupper, Survival of tissue-resident memory T cells requires exogenous lipid uptake and metabolism, *Nature* **543**, 252–256 (2017).

27. T. Duhen, R. Geiger, D. Jarrossay, A. Lanzavecchia, F. Sallusto, Production of interleukin 22 but not interleukin 17 by a subset of human skin-homing memory T cells, *Nat. Immunol.* **10**, 857–863 (2009).

28. S. Trifari, C. D. Kaplan, E. H. Tran, N. K. Crellin, H. Spits, Identification of a human helper T cell population that has abundant production of interleukin 22 and is distinct from T(H)-17, T(H)1 and T(H)2 cells, *Nat. Immunol.* **10**, 864–871 (2009).

29. R. L. Gieseck, M. S. Wilson, T. A. Wynn, Type 2 immunity in tissue repair and fibrosis, *Nat. Rev. Immunol.* **18**, 62–76 (2018).

30. G. F. Sonnenberg, L. A. Fouser, D. Artis, Border patrol: regulation of immunity,

inflammation and tissue homeostasis at barrier surfaces by IL-22, *Nat. Immunol.* **12**, 383–390 (2011).

31. M. Xu, H. Lu, Y.-H. Lee, Y. Wu, K. Liu, Y. Shi, H. An, J. Zhang, X. Wang, Y. Lai, C. Dong, An Interleukin-25-Mediated Autoregulatory Circuit in Keratinocytes Plays a Pivotal Role in Psoriatic Skin Inflammation, *Immunity* **48**, 787-798.e4 (2018).

32. C. K. Wang, C. F. Nelson, A. M. Brinkman, A. C. Miller, W. K. Hoeffler, Spontaneous cell sorting of fibroblasts and keratinocytes creates an organotypic human skin equivalent, *J. Invest. Dermatol.* **114**, 674–680 (2000).

33. E. M. Steinert, J. M. Schenkel, K. A. Fraser, L. K. Beura, L. S. Manlove, B. Z. Igyártó, P. J. Southern, D. Masopust, Quantifying Memory CD8 T Cells Reveals Regionalization of Immunosurveillance, *Cell* **161**, 737–749 (2015).

34. L. K. Beura, S. Wijeyesinghe, E. A. Thompson, M. G. Macchietto, P. C. Rosato, M. J. Pierson, J. M. Schenkel, J. S. Mitchell, V. Vezys, B. T. Fife, S. Shen, D. Masopust, T Cells in Nonlymphoid Tissues Give Rise to Lymph-Node-Resident Memory T Cells, *Immunity* **48**, 327-338.e5 (2018).

35. J. Mohammed, L. K. Beura, A. Bobr, B. Astry, B. Chicoine, S. W. Kashem, N. E. Welty, B. Z. Igyártó, S. Wijeyesinghe, E. A. Thompson, C. Matte, L. Bartholin, A. Kaplan, D. Sheppard, A. G. Bridges, W. D. Shlomchik, D. Masopust, D. H. Kaplan, Stromal cells control the epithelial residence of DCs and memory T cells by regulated activation of TGF-β, *Nat. Immunol.* **17**, 414–421 (2016).

36. A. Toulon, L. Breton, K. R. Taylor, M. Tenenhaus, D. Bhavsar, C. Lanigan, R. Rudolph, J. Jameson, W. L. Havran, A role for human skin–resident T cells in wound healing, *J Exp Med* **206**, 743–750 (2009).

37. C. J. Ferrante, S. J. Leibovich, Regulation of Macrophage Polarization and Wound Healing, *Adv Wound Care (New Rochelle)* **1**, 10–16 (2012).

38. T. Taniguchi, A. M. Woodward, P. Magnelli, N. M. McColgan, S. Lehoux, S. M. P. Jacobo, J. Mauris, P. Argüeso, N-Glycosylation affects the stability and barrier function of the MUC16 mucin, *J. Biol. Chem.* **292**, 11079–11090 (2017).

39. I. K. Gipson, S. Spurr-Michaud, A. Tisdale, B. B. Menon, Comparison of the transmembrane mucins MUC1 and MUC16 in epithelial barrier function, *PLoS ONE* **9**, e100393 (2014).

40. K. McLeod, J. T. Walker, D. W. Hamilton, Galectin-3 regulation of wound healing and fibrotic processes: insights for chronic skin wound therapeutics, *J Cell Commun Signal* **12**, 281–287 (2018).

41. C. M. dos S. Camargo, A. M. Brotas, M. Ramos-e-Silva, S. Carneiro, Isomorphic phenomenon of Koebner: facts and controversies, *Clin. Dermatol.* **31**, 741–749 (2013).

42. G. Weiss, A. Shemer, H. Trau, The Koebner phenomenon: review of the literature, *J Eur Acad Dermatol Venereol* **16**, 241–248 (2002).

43. E. Lebas, F. Libon, A. F. Nikkels, Koebner Phenomenon and Mycosis Fungoides, *Case Rep Dermatol* **7**, 287–291 (2015).

44. R. A. Clark, Resident memory T cells in human health and disease, *Sci Transl Med* **7**, 269rv1 (2015).

45. R. Sanchez Rodriguez, M. L. Pauli, I. M. Neuhaus, S. S. Yu, S. T. Arron, H. W. Harris, S. H.-Y. Yang, B. A. Anthony, F. M. Sverdrup, E. Krow-Lucal, T. C. Mackenzie, D. S. Johnson, E. H. Meyer, A. Löhr, A. Hsu, J. Koo, W. Liao, R. Gupta, M. G. Debbaneh, D. Butler, M. Huynh, E. C. Levin, A. Leon, W. Y. Hoffman, M. H. McGrath, M. D. Alvarado, C. H. Ludwig, H.-A. Truong, M. M. Maurano, I. K. Gratz, A. K. Abbas, M. D. Rosenblum, Memory regulatory T

cells reside in human skin, *J. Clin. Invest.* **124**, 1027–1036 (2014).

46. M. E. Ritchie, B. Phipson, D. Wu, Y. Hu, C. W. Law, W. Shi, G. K. Smyth, limma powers differential expression analyses for RNA-sequencing and microarray studies, *Nucleic Acids Res.* **43**, e47 (2015).

47. H. S. Robins, P. V. Campregher, S. K. Srivastava, A. Wacher, C. J. Turtle, O. Kahsai, S. R. Riddell, E. H. Warren, C. S. Carlson, Comprehensive assessment of T-cell receptor beta-chain diversity in alphabeta T cells, *Blood* **114**, 4099–4107 (2009).

48. M. A. Merkley, E. Hildebrandt, R. H. Podolsky, H. Arnouk, D. G. Ferris, W. S. Dynan, H. Stöppler, Large-scale analysis of protein expression changes in human keratinocytes immortalized by human papilloma virus type 16 E6 and E7 oncogenes, *Proteome Sci* **7**, 29 (2009).

49. J. M. Daley, A. A. Thomay, M. D. Connolly, J. S. Reichner, J. E. Albina, Use of Ly6G-specific monoclonal antibody to deplete neutrophils in mice, *J. Leukoc. Biol.* **83**, 64–70 (2008).

50. W. J. Racki, L. Covassin, M. Brehm, S. Pino, R. Ignotz, R. Dunn, J. Laning, S. K. Graves, A. A. Rossini, L. D. Shultz, D. L. Greiner, NOD-scid IL2rγnull (NSG) Mouse Model of Human Skin Transplantation and Allograft Rejection, *Transplantation* **89**, 527–536 (2010).

51. I. K. Gratz, M. D. Rosenblum, M. M. Maurano, J. S. Paw, H.-A. Truong, A. Marshak-Rothstein, A. K. Abbas, Cutting edge: Self-antigen controls the balance between effector and regulatory T cells in peripheral tissues, *J. Immunol.* **192**, 1351–1355 (2014).

Acknowledgements

We thank Dr. A. Sir and Dr. R. Reitsamer of the Breast Center of the University Hospital Salzburg, Paracelsus Medical University Salzburg, Austria for providing us with skin and blood samples. We also thank Anna Hochreiter, MSc, and Anna Raninger, MSc, from the Flow Cytometry Core facility at the Cell Therapy Institute, PMU Salzburg. We thank Dr. Stefan Hainzl, EB House Austria, Department of Dermatology, University Hospital of the Paracelsus Medical University Salzburg, Austria, for the immortalization of primary human keratinocytes and fibroblasts. We further thank Ariane Benedetti for technical assistance and for performing the skin histology. In Seattle, we thank Kassidy Benoscek and Florence Roan for help in obtaining skin and blood samples, Thien Son-Nguyen for frozen PBMC, Alice Weidemann for help with CyTOF, Vivian Gersuk for help with RNA-seq, and Scott Presnell, Matt Dufort and Hannah DeBerg for helpful discussions on RNA-seq analysis. **Funding**: This work was supported by the Focus Program "ACBN" of the University of Salzburg, Austria, and NIH grant R01AI127726 awarded to IKG and DJC. MMK is part of the PhD program Immunity in Cancer and Allergy, funded by the Austrian Science Fund (FWF, grant W 1213) and was recipient of a DOC Fellowship of the Austrian Academy of Sciences. **Competing interests**: The authors have no conflicts of interest to report. **Data and materials availability**: Raw and processed RNA-seq data can be found in Supplementary Data Excel Files 1 and 2. Immediately upon publication, RNA-seq data will be deposited in the gene expression omnibus (GEO), and CyTOF data will be made available at flowrepository.org

Author contributions: M.M.K., P.A.M., B.H., S.R.V., T.D., D.J.C. and I.K.G. designed the experiments; M.M.K., M.D.R. and I.K.G. developed xenografting methods; M.M.K., P.A.M., B.H., S.R.V., S.M. and T.D. performed experiments; B.H. performed computational analysis; S.A.L. helped develop the CyTOF panels; G.B. helped set up the sort panels; D.J.C. and I.K.G. wrote the manuscript; M.M.K., P.A.M., B.H., S.V., S.M., T.D. and M.D.R. reviewed and edited the paper; D.J.C. and I.K.G. supervised the project.

Figure legends

Figure 1: CLA$^+$CD103$^+$ T cells downregulate CD69 and exit the skin. (**A**) Representative flow cytometry analysis of CD69 and CD103 expression by gated CD8$^+$ and CD4$^+$ T cells from human skin. (**B**) Graphical summary of the proportions of CD69- and CD103-defined T cell populations among CD8$^+$ and CD4$^+$ skin T cells. (**C**) Representative flow cytometry analysis of CLA expression by gated CD103$^+$CD69$^+$ T_{RM} in human skin. (**D**), Human skin was adhered to tissue culture plates and cultured for 7 days submerged in media. The ratio of CD4$^+$ and CD8$^+$ T cells and the expression of CLA and CD103 by T cells in the indicated samples were analyzed by flow cytometry. Representative data (N=4). (**E**) Graphical summary of the proportion of CD69$^-$ cells among CD4$^+$CLA$^+$CD103$^+$ T cells from the indicated samples. Open symbols represent data from a subject with mammary carcinoma but no skin condition. Significance determined by paired, two-tailed students t-test. (**F**) Three 8mm-punch biopsies of healthy human skin per animal (N=3) were placed on the back of NSG mice and grafts as well as spleens were analyzed by flow cytometry 50 days later. Representative flow cytometry analysis of CLA and CD103 expression by live gated human CD45$^+$CD3$^+$CD4$^+$CD25$^-$CD45RA$^-$ T cells. **(G)**

Graphical summary showing CD103 expression by live gated human $CD45^+CD3^+CD4^+CD25^-CD45RA^-CLA^+$ T cells from skin grafts and spleens of skin-grafted NSG mice.

Figure 2: CLA^+CD103^+ T cells constitute a unique cell population in human blood. (**A**) (Left), Mass cytometry analysis of CD45RA and CLA expression by gated $CD3^+CD45^+$ PBMC showing the gate used to define $CD3^+CLA^+$ T cells for subsequent clustering analysis. (Right), tSNE analysis and clustering of $CD3^+CLA^+$ T cells from blood of 5 healthy donors based on expression of CD4, CD8, CCR7, CD103, β7Integrin, CXCR3, CCR6, CCR4, CCR10, Foxp3, CD27, β7 integrin, CD25, CD161, and CD56. (**B**) Heat map showing relative expression of the indicated markers in each of the $CD3^+CLA^+$ cell clusters. (**C**) tSNE analysis of $CD3^+CLA^+$ T cells overlaid with relative expression of the indicated markers.

Figure 3: Shared phenotype of CLA^+CD103^+ T cells from human blood and skin. (**A**) Representative flow cytometry analysis of CD45RA and CLA expression by gated $CD4^+$ T cells from blood and skin of healthy donors. (**B**) Representative flow cytometry analysis of CCR7 and CD103 expression by gated $CD4^+CD45RA^-CLA^+$ memory T cells from PBMC and skin of healthy donors. **c**, Graphical summary of the proportions of CCR7- and CD103-defined T cell populations among $CD4^+CD45RA^-CLA^+$ cells from blood and skin. (**D,E**) Representative flow cytometry analysis and graphical summary of expression of the indicated markers by $CD4^+$ T cell populations in the blood and skin as indicated. Significance determined by one-way repeated measures ANOVA with Tukey's post-test for pairwise comparisons.

Figure 4: CLA^+CD103^+ T cells from human blood and skin share a transcriptional profile. Whole transcriptome profiling by RNA-sequencing was performed on sorted CLA^+ T cell subsets from blood or skin. (**A**) Venn diagram showing the number of significantly differentially

expressed (DE) genes (FDR<0.05 and log2 fold-change >1) between CLA^+CD103^+ T cells and either $CLA^+CD103^-CCR7^+$ or $CLA^+CD103^-CCR7^-$ T cells as indicated. The overlapping 83 genes were designated the $CD103^+$ gene signature. (**B**) Barcode plot showing the distribution of the $CD103^+$ signature genes (red=up- blue=down-regulated in $CD103^+$) relative to gene expression changes comparing $CD103^+$ and $CD103^-CCR7^-$ T cells from the blood or skin as indicated. Significance determined by rotation gene set testing for linear models. (**C**) Heat map and hierarchical clustering of RNA-seq samples from the indicated blood and skin cell populations based on the $CD103^+$ gene signature. (**D**) PCA analysis of RNA-seq samples from the indicated blood and skin cell populations based on the $CD103^+$ gene signature or on 83 randomly selected genes. (**E**) PCA analysis of RNA-seq samples from $CD4^+CD69^+$ and $CD4^+CD69^-$ T cell populations from lung and spleen (data from GEO dataset GSE94964*(3)*) based on the $CD103^+$ gene signature or 83 randomly selected genes. (**F**) Venn diagram showing functional annotation of key genes up- or down-regulated by CLA^+CD103^+ T cells in blood or skin identified in our phenotypic, functional, and transcriptional analyses. Underlined gene names indicate proteins whose expression pattern was validated by flow cytometry in Figs 3 and 5.

Figure 5: CLA^+CD103^+ T cells from human blood and skin share a functional profile. (**A**) Representative flow cytometry analysis of CD45RA and CLA expression by gated $CD4^+$ T cells from blood and skin of healthy donors. (**B,C,D**) Representative flow cytometry analysis of indicated CLA/CD103 subpopulations of blood and skin $CD4^+CD45RA^-$ cells producing IL-13, IL-4, IL-22, IL-17A, IFN-γ and GM-CSF as indicated upon *ex vivo* stimulation with PMA/ionomycin and intracellular cytokine staining. (**E**) Graphical summary of the proportions of CLA^-CD103^-, CLA^+CD103^-, and CLA^+CD103^+ $CD4^+CD45RA^-$ cells producing cytokines as

indicated. Open symbols represent data from a subject with mammary carcinoma. Significance determined by one-way repeated measures ANOVA with Tukey's post-test for pairwise comparisons.

Figure 6: CLA$^+$CD103$^+$ T cells in skin and blood are clonally related. TCRβ-sequencing was performed on CLA$^+$ T cell subsets from blood and skin sorted based on expression of CD103 and CCR7 as indicated. (**A**) (left) Circle plot of unique productive TCRβ sequences from each of the indicated populations of CLA$^+$ T cells from one representative donor. Connections highlight sequences from skin CLA$^+$CD103$^+$ cells found in each of the other populations. For visualization, sequences were downsampled (weighted for relative abundance) for populations containing >1000 unique sequences. (right) Graphical summary of the Morisita index as a measure of TCR repertoire similarity over all productive rearrangements between CLA$^+$CD103$^+$ cells in the blood and each of the indicated populations across all 4 donors examined. (**B**) Circle plot (left) and graphical summary of the Morisita index (right) as in **A** using CLA$^+$CD103$^+$ T cells from blood as the reference population. Significance determined by one-way ANOVA with Dunnett's multiple comparisons test.

Figure 7: CLA$^+$CD103$^+$ T$_{RM}$ can exit the skin and reseed distant skin sites in a xenograft model. (**A**) *In vitro* expanded human keratinocytes and fibroblasts were grafted onto the backs of NSG mice using a grafting chamber. After 99 days of healing and differentiation, the engineered skin or adjacent murine skin were excised, frozen in OCT and stained either with hematoxylin and eosin (left) or with anti-human type VII collagen prior to immunofluorescence analysis (right). Human skin from a healthy donor was used as control. (**B**) Experimental schematic for the generation of engineered skin (ES) followed by xenografting human skin onto NSG mice.

(**C**) Representative photograph of ES and skin grafts on day 144. (**D**) Representative flow cytometry analysis and (**E**) graphical summary of CLA^+CD103^+ cells by live gated human $CD45^+CD3^+CD4^+CD45RA^-$ T cells from skin grafts, spleen, and ES (3-5 weeks after skin grafting). Open and filled symbols denote samples derived from 2 different skin donors. Each symbol represents data from one recipient animal. (**F**) Representative flow cytometry analysis and graphical summary of expression of CD27, CD9 and CD69 by gated $CD45^+CD4^+CD45RA^-CD103^+CLA^+$ T cells in the skin grafts, spleen, and ES 5 weeks after skin grafting (day 145 relative to ES generation). Significance determined by one-way ANOVA with Tukey's post-test for pairwise comparisons. (**G**) Experimental schematic for the generation of engineered skin (ES) followed by adoptive transfer of $2.5x10^6$ PBMC (autologous to the ES)/mouse into NSG mice. (**H**) Representative flow cytometry analysis and (**I**) graphical summary of CLA^+CD103^+ cells by live gated human $CD45^+CD3^+CD4^+CD45RA^-$ T cells from spleen, and ES 25 days after PBMC transfer. Each symbol represents data from one recipient animal. Significance determined by paired t-test.

Figure 1

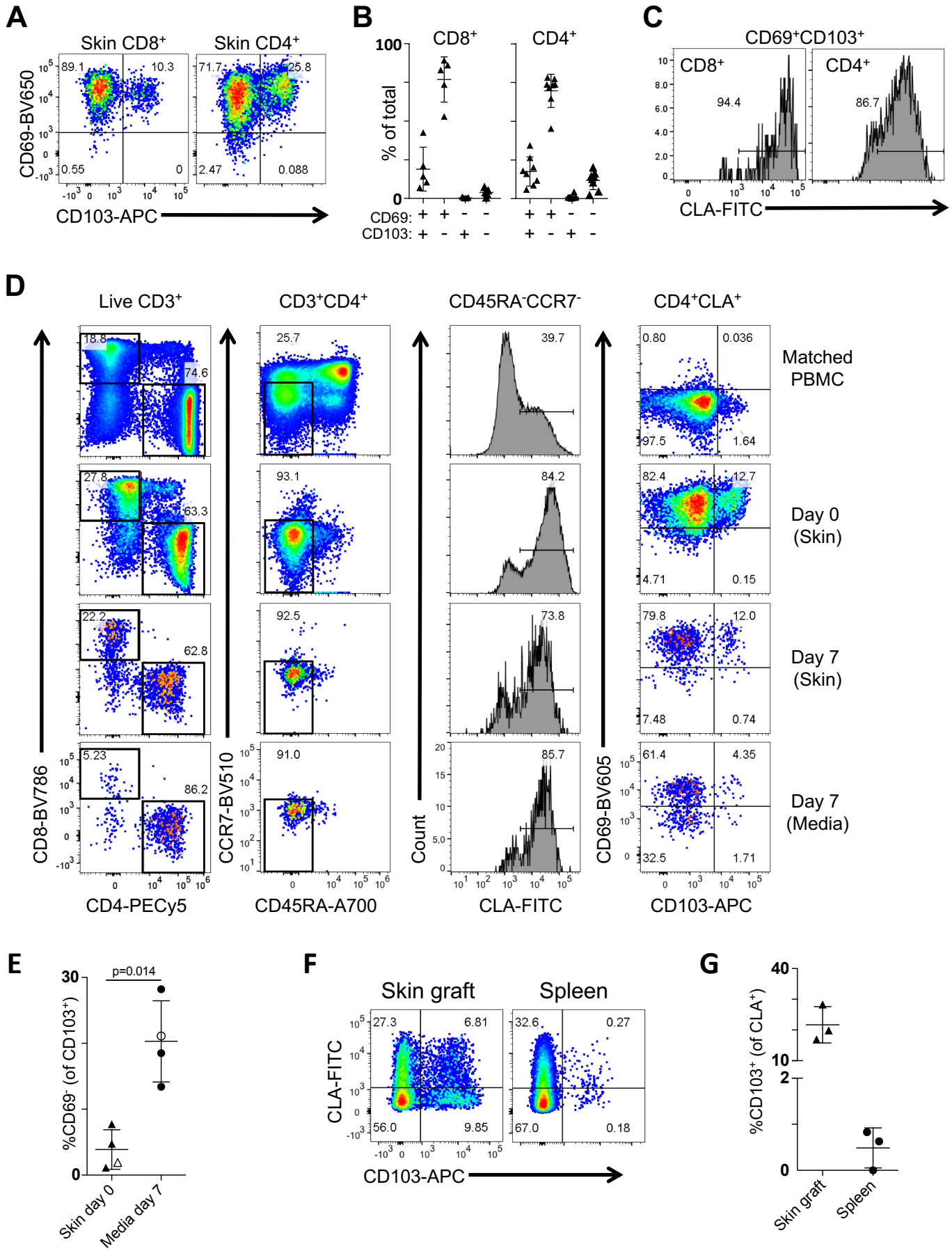
A
Skin CD8+
Skin CD4+
CD69-BV650
CD103-APC
89.1
10.3
0.55
0
71.7
25.8
2.47
0.088
B
CD8+
CD4+
% of total
100
0
CD69: + + - - + + - -
CD103: + - + - + - + -
C
CD69+CD103+
CD8+
CD4+
94.4
86.7
CLA-FITC
D
Live CD3+
CD3+CD4+
CD45RA-CCR7-
CD4+CLA+
Matched PBMC
Day 0 (Skin)
Day 7 (Skin)
Day 7 (Media)
18.8
74.6
25.7
39.7
0.80
0.036
97.5
1.64
27.8
63.3
93.1
84.2
82.4
12.7
4.71
0.15
22.2
62.8
92.5
73.8
79.8
12.0
7.48
0.74
5.23
86.2
91.0
85.7
61.4
4.35
32.5
1.71
CD8-BV786
CD4-PECy5
CCR7-BV510
CD45RA-A700
Count
CLA-FITC
CD69-BV605
CD103-APC
E
p=0.014
%CD69- (of CD103+)
30
0
Skin day 0
Media day 7
F
Skin graft
Spleen
CLA-FITC
CD103-APC
27.3
6.81
56.0
9.85
32.6
0.27
67.0
0.18
G
%CD103+ (of CLA+)
40
10
2
0
Skin graft
Spleen

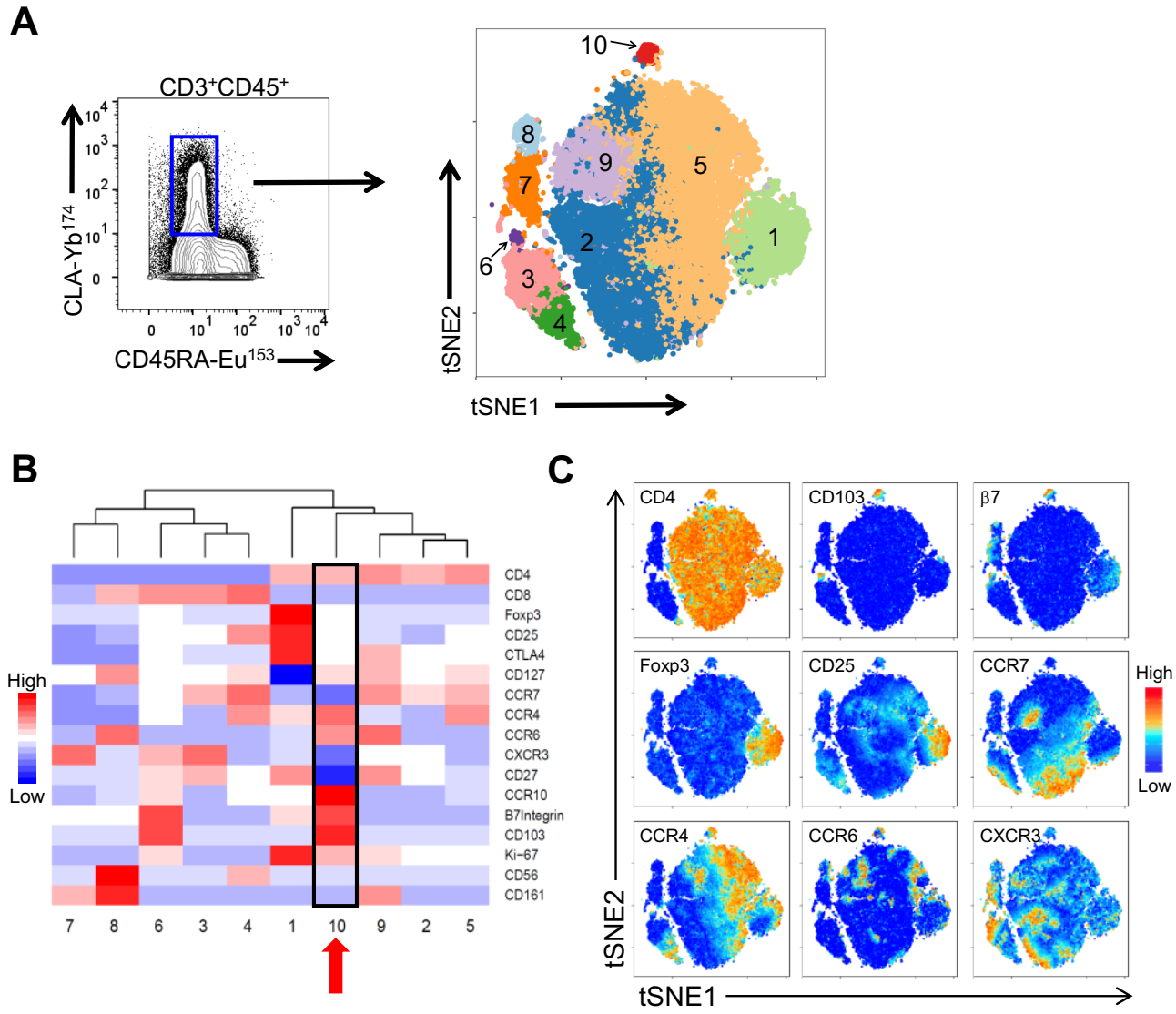
A
CD3+CD45+
CLA-Yb174
CD45RA-Eu153
tSNE2
tSNE1
10
8
9
5
7
2
1
6
3
4
B
High
Low
CD4
CD8
Foxp3
CD25
CTLA4
CD127
CCR7
CCR4
CCR6
CXCR3
CD27
CCR10
B7Integrin
CD103
Ki-67
CD56
CD161
7 8 6 3 4 1 10 9 2 5
C
CD4
CD103
β7
Foxp3
CD25
CCR7
CCR4
CCR6
CXCR3
High
Low
tSNE2
tSNE1

Figure 3

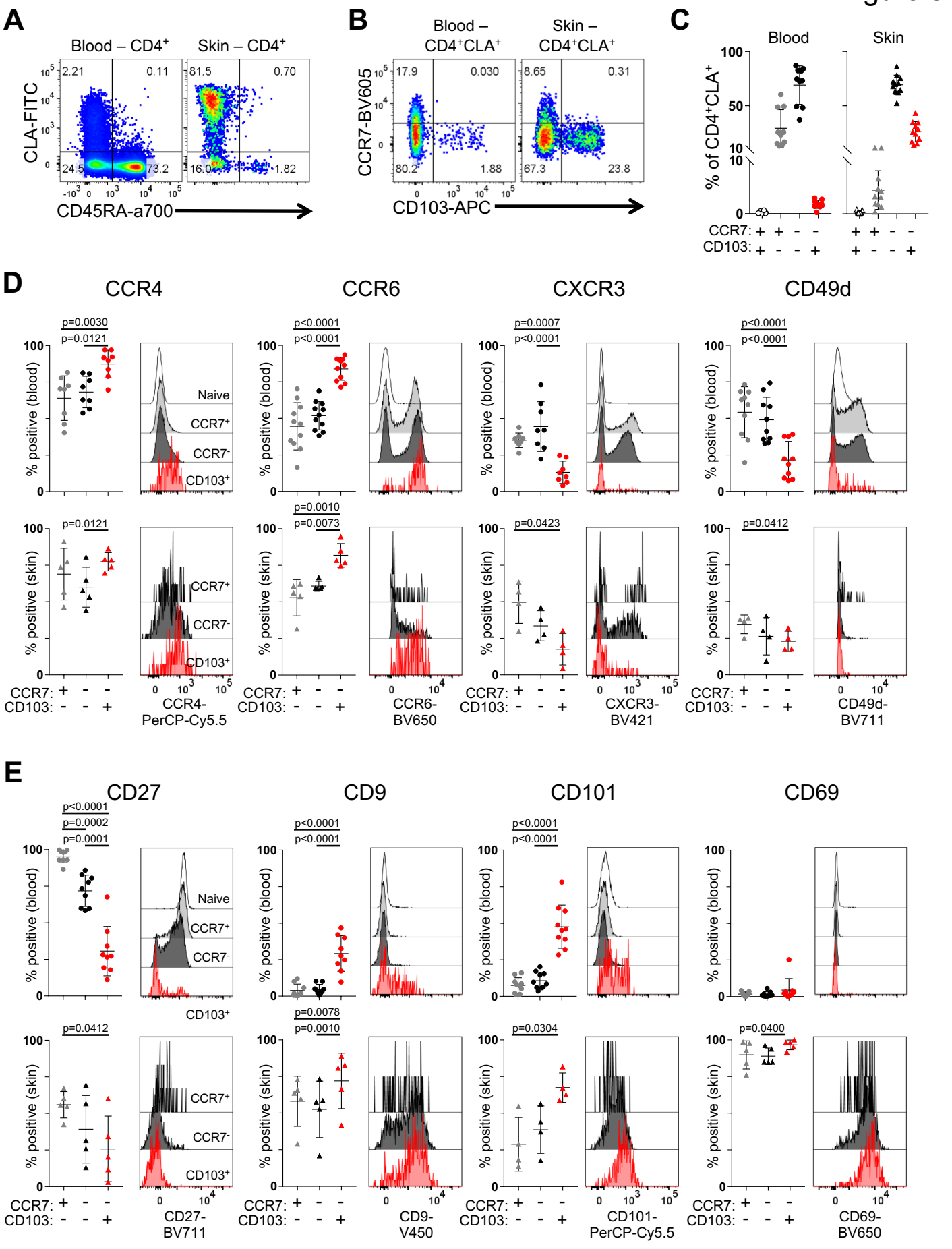
A
Blood – CD4+
Skin – CD4+
CLA-FITC
CD45RA-a700
2.21
0.11
24.5
73.2
81.5
0.70
16.0
1.82
B
Blood – CD4+CLA+
Skin – CD4+CLA+
CCR7-BV605
CD103-APC
17.9
0.030
80.2
1.88
8.65
0.31
67.3
23.8
C
Blood
Skin
% of CD4+CLA+
CCR7:
CD103:
D
CCR4
CCR6
CXCR3
CD49d
% positive (blood)
% positive (skin)
p=0.0030
p=0.0121
p<0.0001
p<0.0001
p=0.0007
p<0.0001
p<0.0001
p<0.0001
p=0.0121
p=0.0010
p=0.0073
p=0.0423
p=0.0412
Naive
CCR7+
CCR7-
CD103+
CCR4-PerCP-Cy5.5
CCR6-BV650
CXCR3-BV421
CD49d-BV711
E
CD27
CD9
CD101
CD69
p<0.0001
p=0.0002
p=0.0001
p<0.0001
p<0.0001
p<0.0001
p<0.0001
p=0.0412
p=0.0078
p=0.0010
p=0.0304
p=0.0400
CD27-BV711
CD9-V450
CD101-PerCP-Cy5.5
CD69-BV650

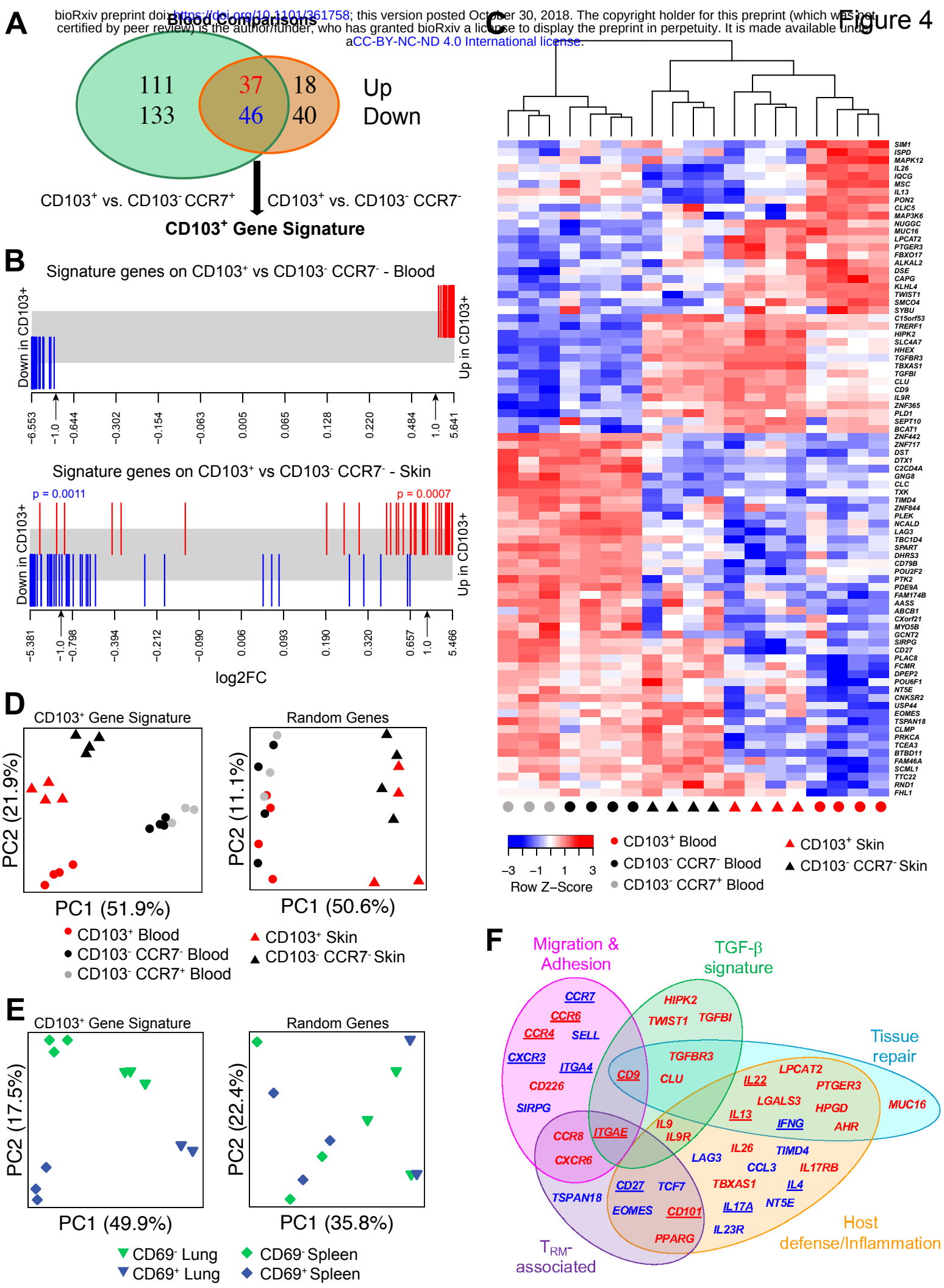

Figure 5

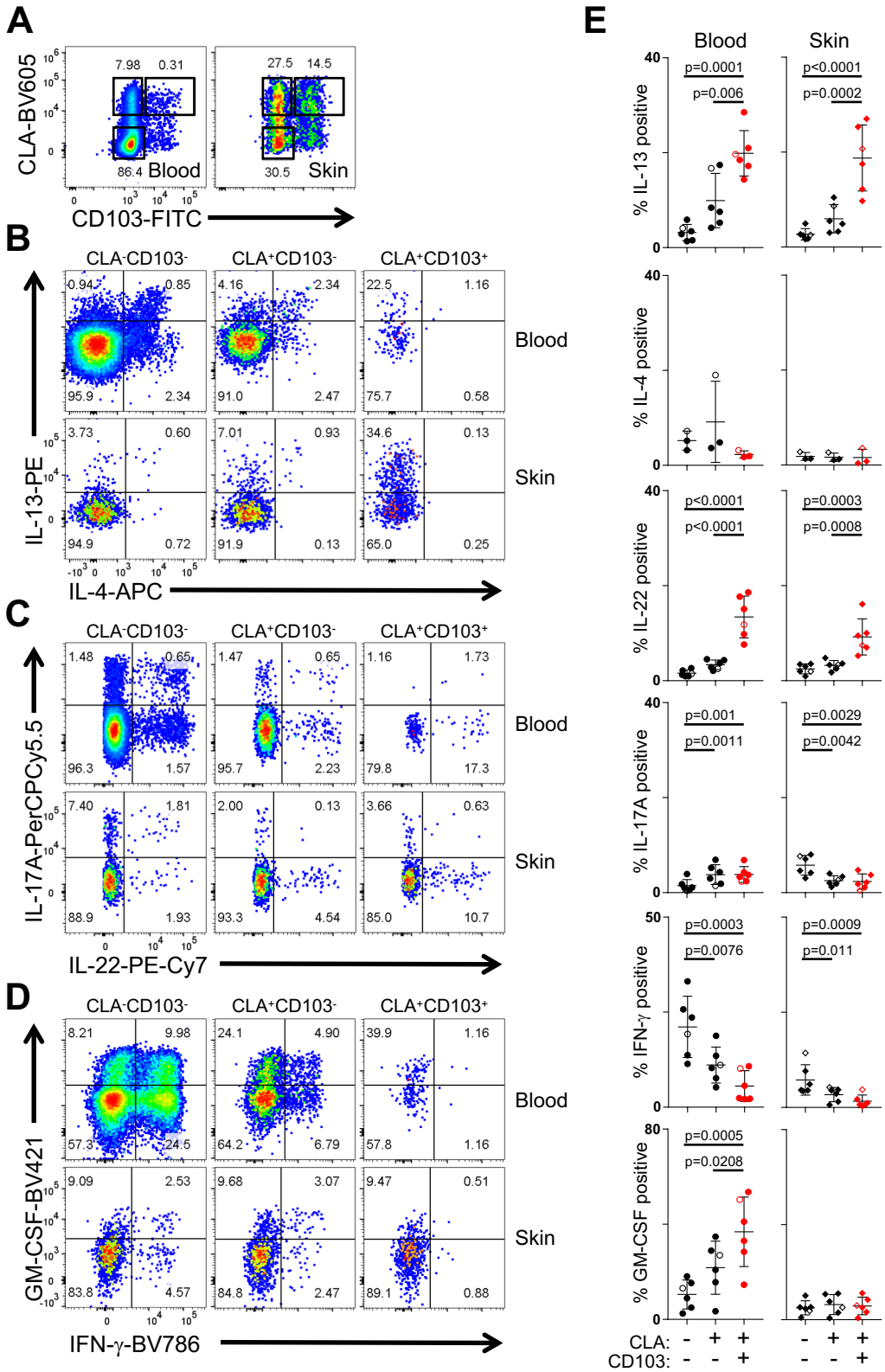
A
CLA-BV605
CD103-FITC
7.98
0.31
86.4
Blood
27.5
14.5
30.5
Skin
B
CLA-CD103-
CLA+CD103-
CLA+CD103+
Blood
Skin
IL-13-PE
IL-4-APC
0.94
0.85
95.9
2.34
4.16
2.34
91.0
2.47
22.5
1.16
75.7
0.58
3.73
0.60
94.9
0.72
7.01
0.93
91.9
0.13
34.6
0.13
65.0
0.25
C
IL-17A-PerCPCy5.5
IL-22-PE-Cy7
1.48
0.65
96.3
1.57
1.47
0.65
95.7
2.23
1.16
1.73
79.8
17.3
7.40
1.81
88.9
1.93
2.00
0.13
93.3
4.54
3.66
0.63
85.0
10.7
D
GM-CSF-BV421
IFN-γ-BV786
8.21
9.98
57.3
24.5
24.1
4.90
64.2
6.79
39.9
1.16
57.8
1.16
9.09
2.53
83.8
4.57
9.68
3.07
84.8
2.47
9.47
0.51
89.1
0.88
E
Blood
Skin
% IL-13 positive
p=0.0001
p=0.006
p<0.0001
p=0.0002
% IL-4 positive
% IL-22 positive
p<0.0001
p<0.0001
p=0.0003
p=0.0008
% IL-17A positive
p=0.001
p=0.0011
p=0.0029
p=0.0042
% IFN-γ positive
p=0.0003
p=0.0076
p=0.0009
p=0.011
% GM-CSF positive
p=0.0005
p=0.0208
CLA: - + + - + +
CD103: - - + - - +

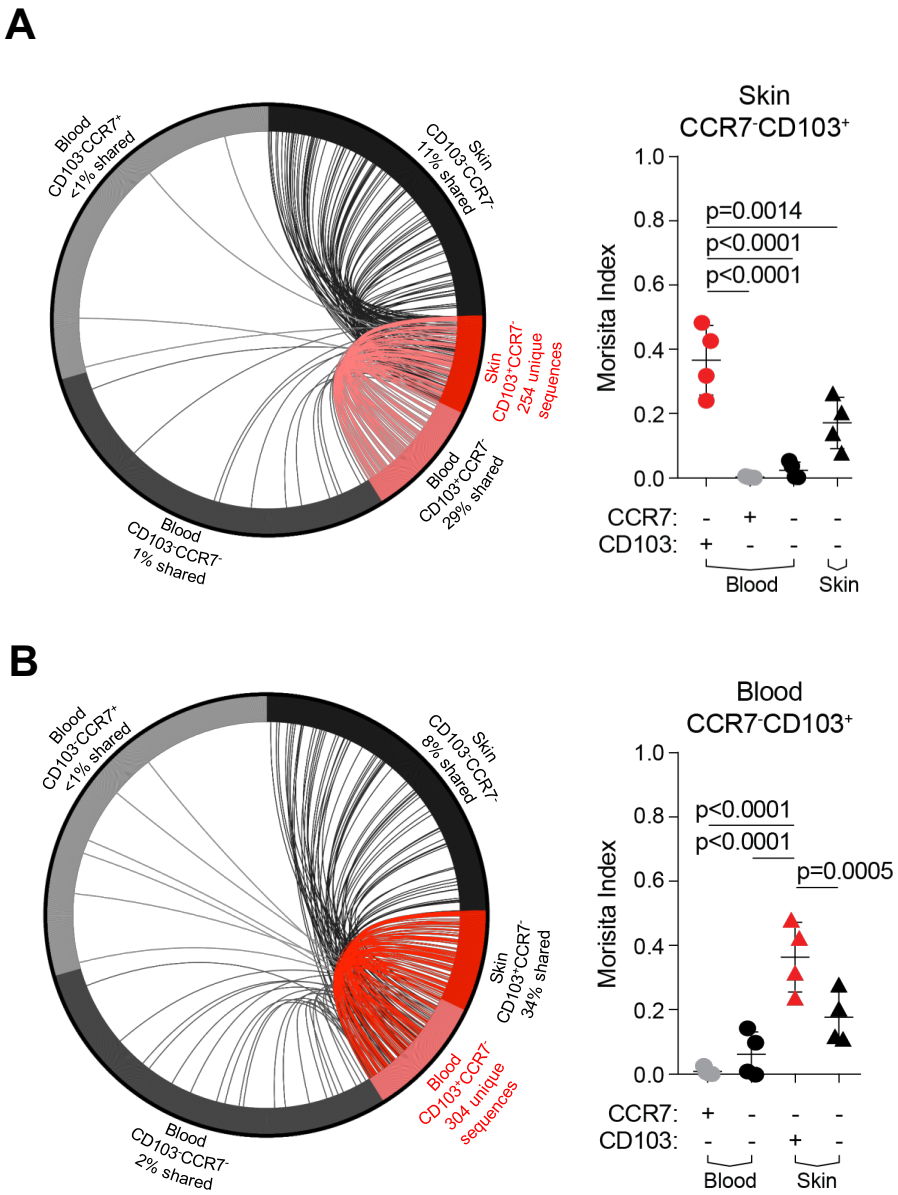
A
Blood CD103-CCR7+ <1% shared
Skin CD103-CCR7- 11% shared
Skin CD103+CCR7- 254 unique sequences
Blood CD103+CCR7- 29% shared
Blood CD103-CCR7- 1% shared
Skin CCR7-CD103+
Morisita Index
p=0.0014
p<0.0001
p<0.0001
CCR7:
CD103:
Blood
Skin
B
Blood CD103-CCR7+ <1% shared
Skin CD103-CCR7- 8% shared
Skin CD103+CCR7- 34% shared
Blood CD103+CCR7- 304 unique sequences
Blood CD103-CCR7- 2% shared
Blood CCR7-CD103+
Morisita Index
p<0.0001
p<0.0001
p=0.0005
CCR7:
CD103:
Blood
Skin

Figure 7

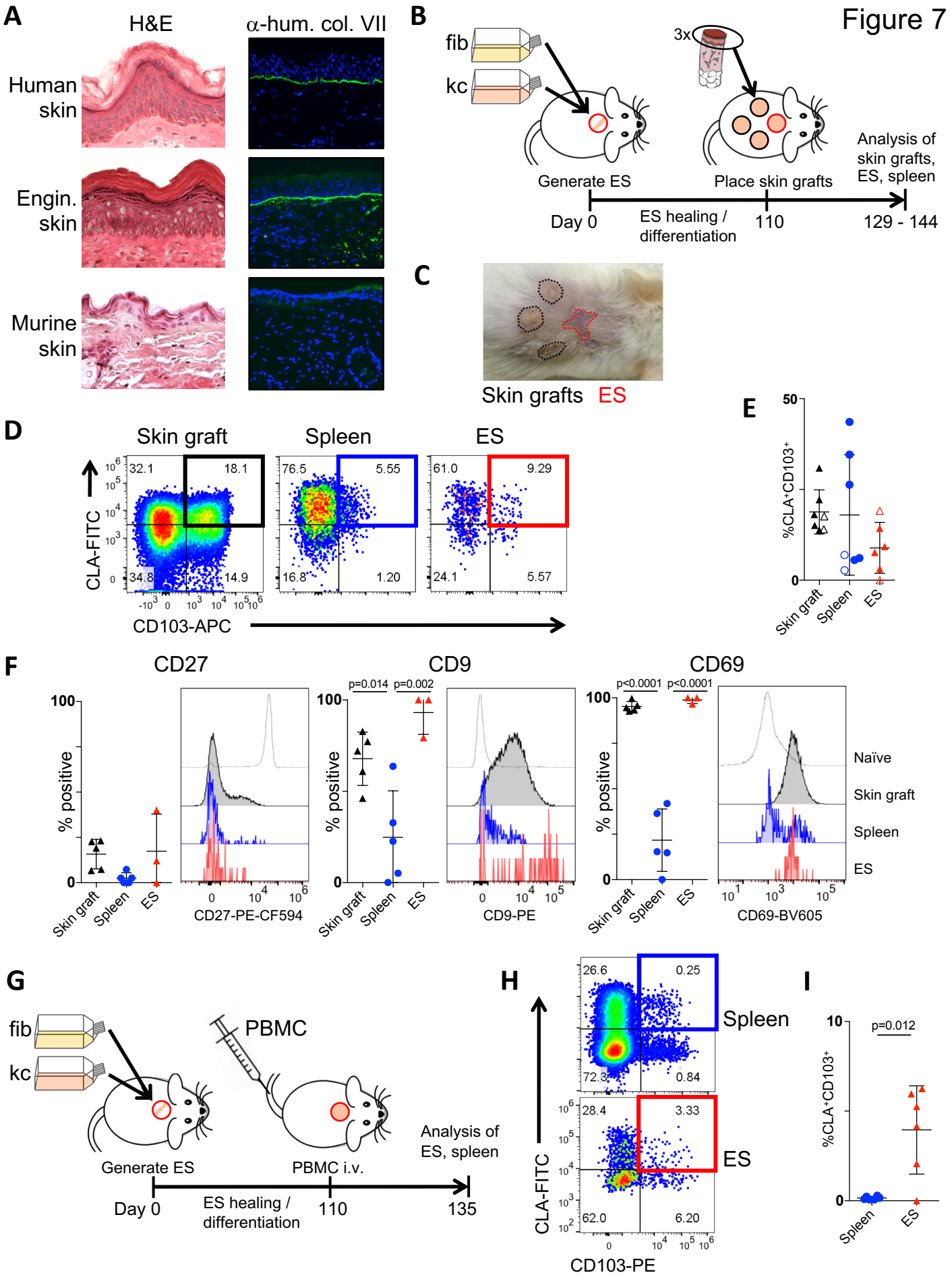
A
H&E
α-hum. col. VII
Human skin
Engin. skin
Murine skin
B
fib
kc
3x
Generate ES
Place skin grafts
Analysis of skin grafts, ES, spleen
Day 0
ES healing / differentiation
110
129 - 144
C
Skin grafts ES
D
Skin graft
Spleen
ES
CLA-FITC
CD103-APC
32.1
18.1
34.8
14.9
76.5
5.55
16.8
1.20
61.0
9.29
24.1
5.57
E
%CLA+CD103+
Skin graft
Spleen
ES
F
CD27
CD9
CD69
% positive
p=0.014
p=0.002
p<0.0001
p<0.0001
CD27-PE-CF594
CD9-PE
CD69-BV605
Naïve
Skin graft
Spleen
ES
G
fib
kc
PBMC
Generate ES
PBMC i.v.
Analysis of ES, spleen
Day 0
ES healing / differentiation
110
135
H
26.6
0.25
72.3
0.84
28.4
3.33
62.0
6.20
Spleen
ES
CLA-FITC
CD103-PE
I
%CLA+CD103+
p=0.012
Spleen
ES

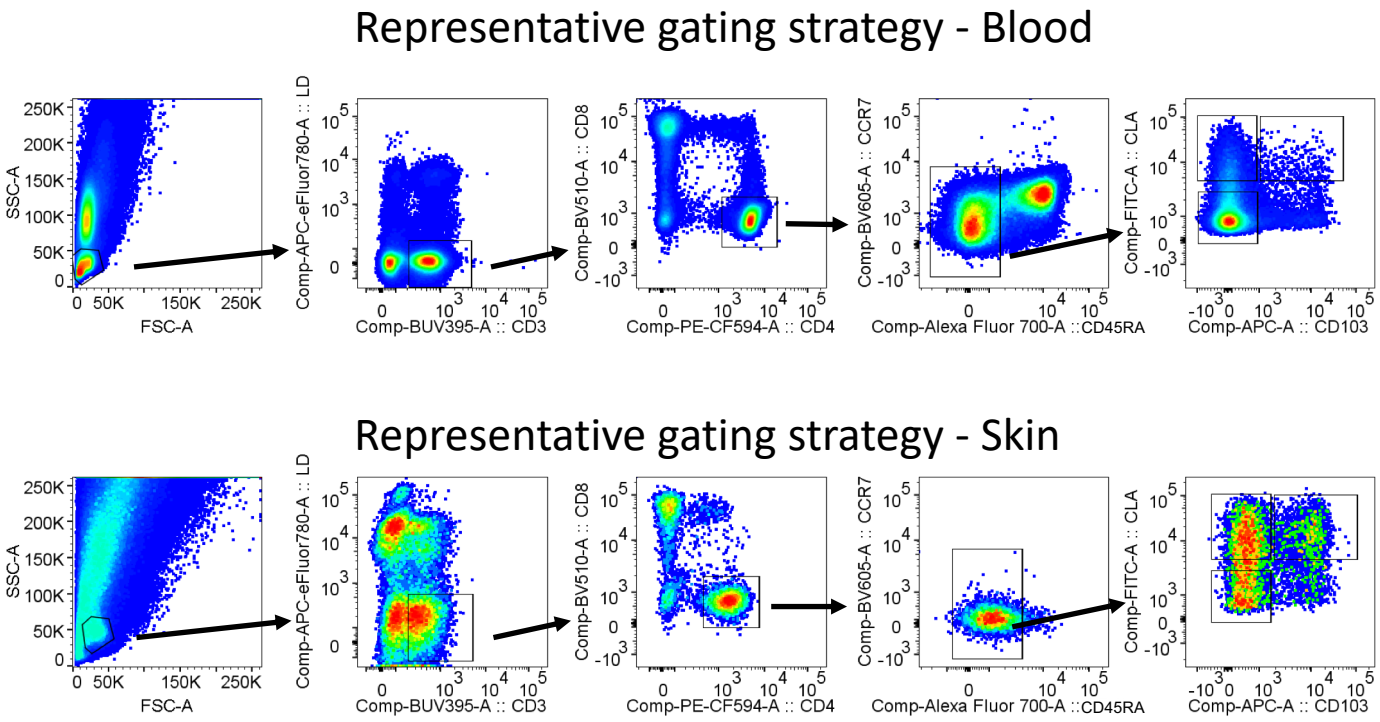

Fig. S1: Representative flow cytometry gating strategies used to identify T cell subsets in human blood and skin.

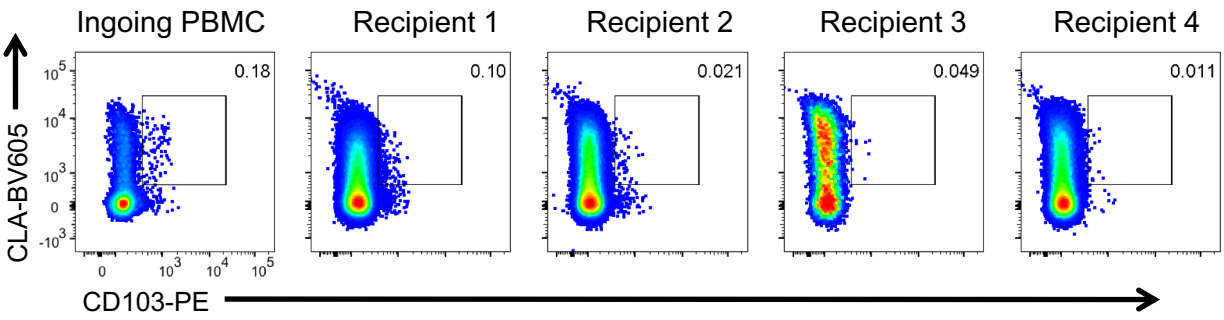

Fig. S2: CD103 expression is not induced on human CD4⁺ T cells in NSG mice. $3x10^6$ PBMC were transferred into NSG mice and the spleens were analyzed by flow cytometry 49 days later. Representative flow cytometry analysis of CLA and CD103 expression by gated $CD4^+CD45^+$ T cells in the ingoing transferred PBMC and in cells recovered from the spleen of four individual recipients.

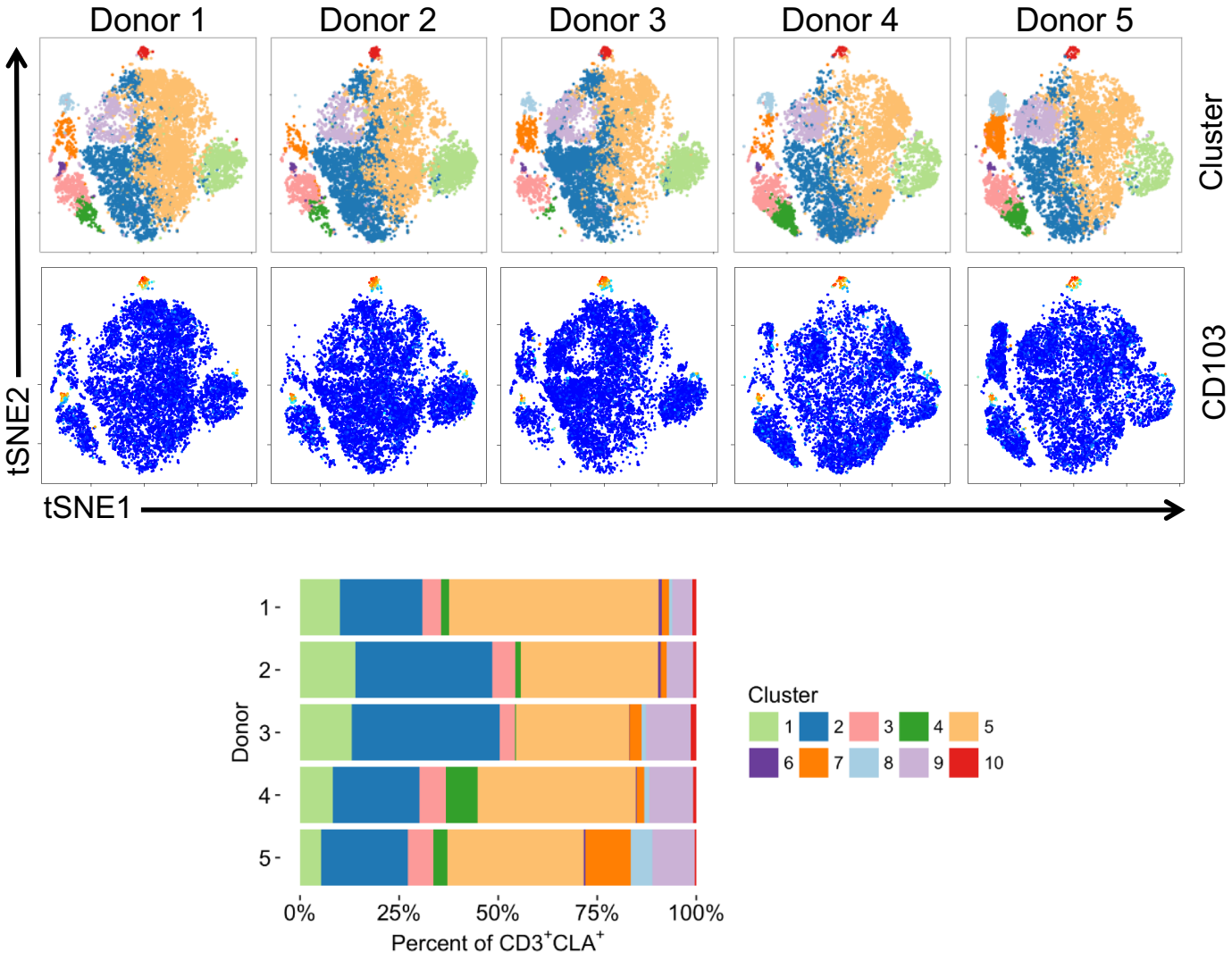

Fig. S3: CyTOF analysis of CLA⁺ T cells in PBMC. (Top) tSNE analysis of gated $CD3^{+}CLA^{+}$ T cells from 5 individual donors showing clustering or CD103 expression as indicated. (Bottom) Stacked bar graph showing the frequency of cells in each of the 10 tSNE-defined clusters in each of the 5 donors examined.

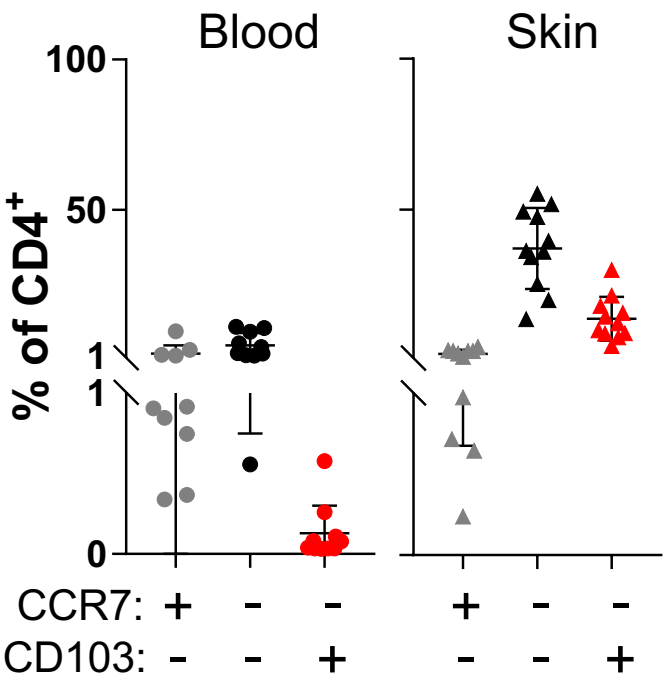

Fig. S4: Frequencies of CLA$^+$ T cell subsets in blood and skin. Graphical summary of the proportions of CLA$^+$CCR7$^+$CD103$^-$, CLA$^+$CCR7$^-$CD103$^-$, and CLA$^+$CCR7$^-$CD103$^+$ T cells among CD4$^+$ T cells from blood and skin.

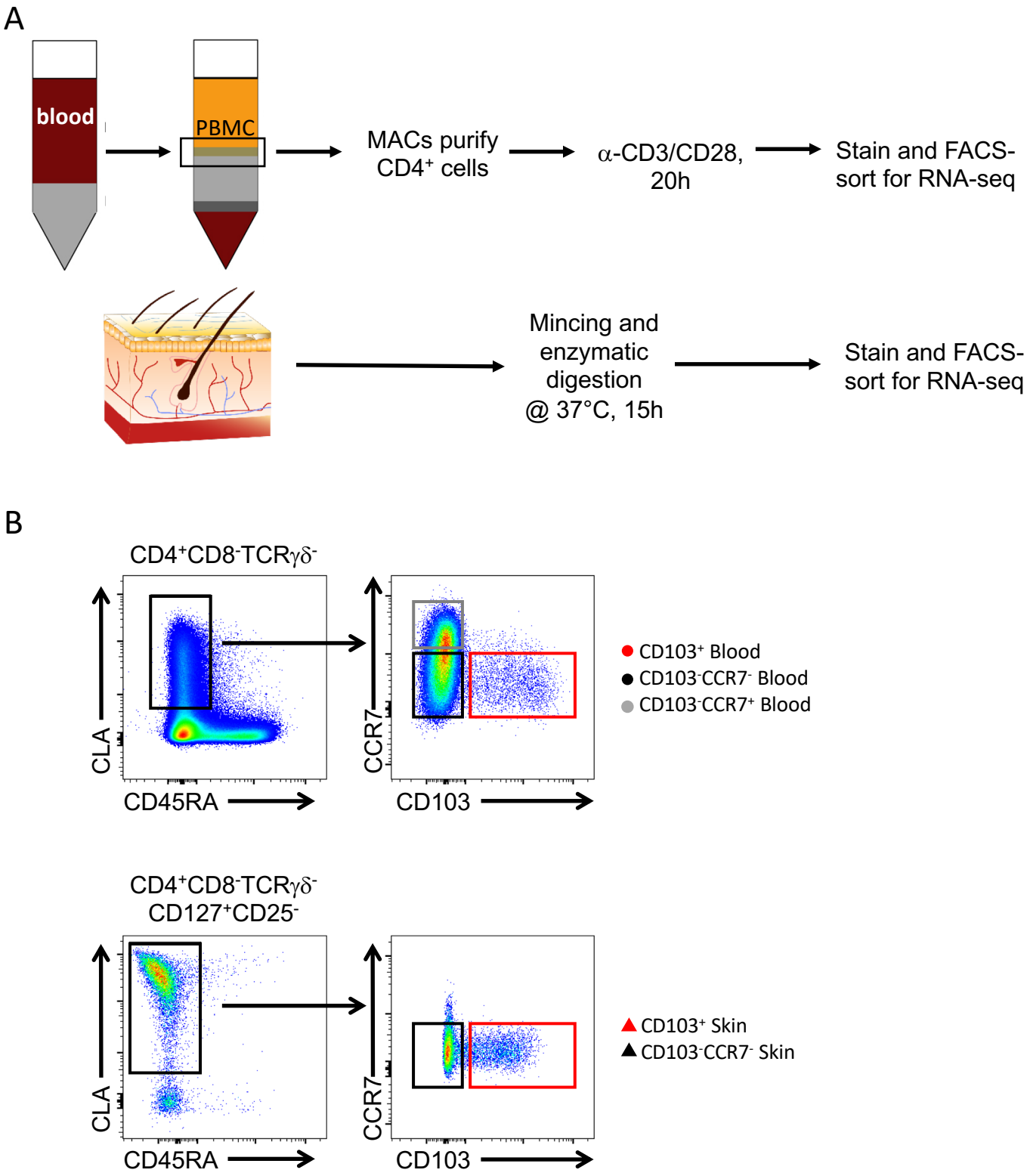

Fig. S5: Experimental schematic of cell isolation and sort gates for RNA-seq. (**A**) Experimental schematic for processing and sorting of T cells from blood and skin for RNA-seq analysis. (**B**) Representative flow cytometry analysis of T cells isolated from blood or skin showing approximate gates used to sort the indicated populations for RNA-seq analysis.

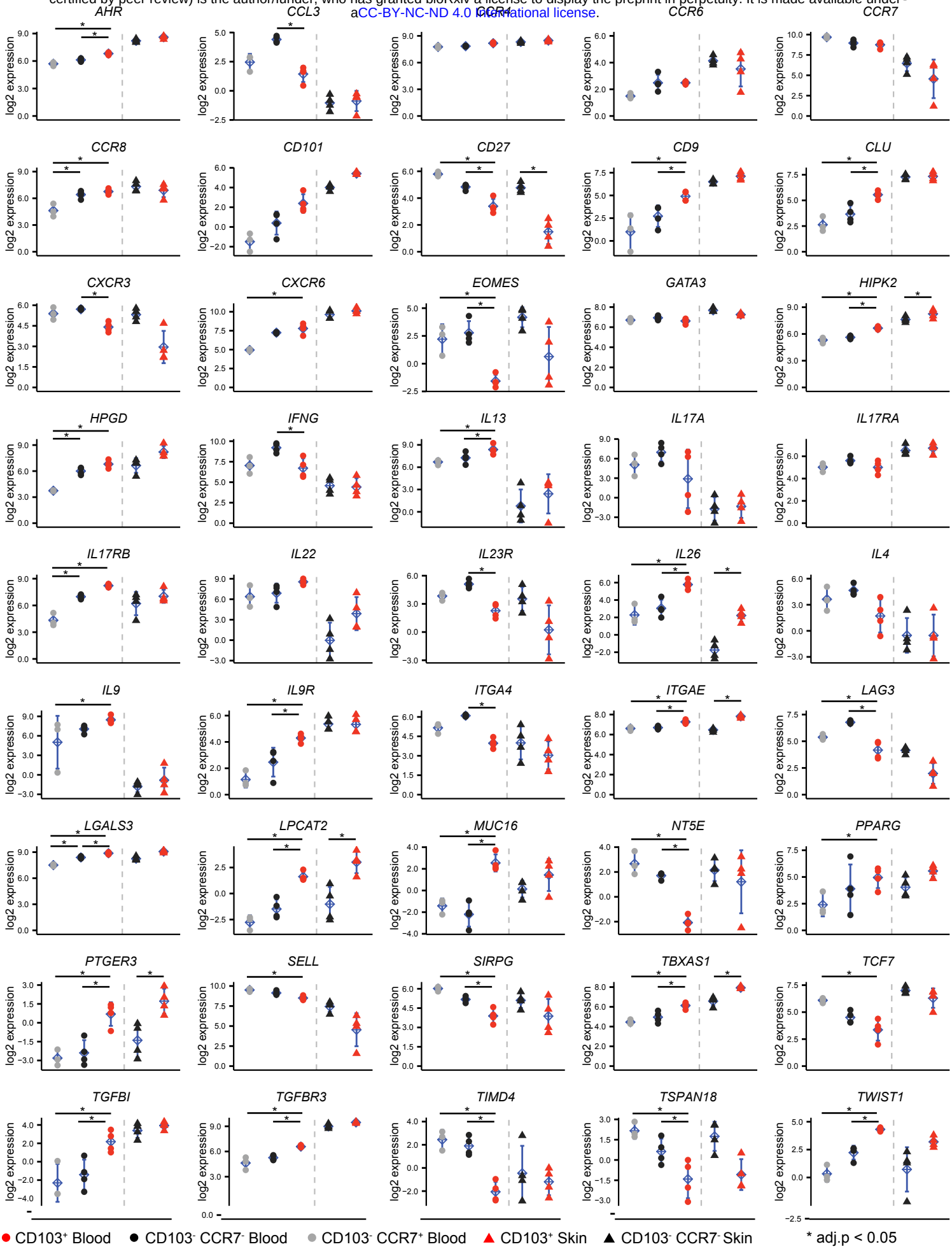

Fig. S6: Expression of selected genes in sorted CD4⁺CLA⁺ T cells from blood and skin. Adjusted p.value computed by fitting a linear model with the displayed comparisons as contrasts.

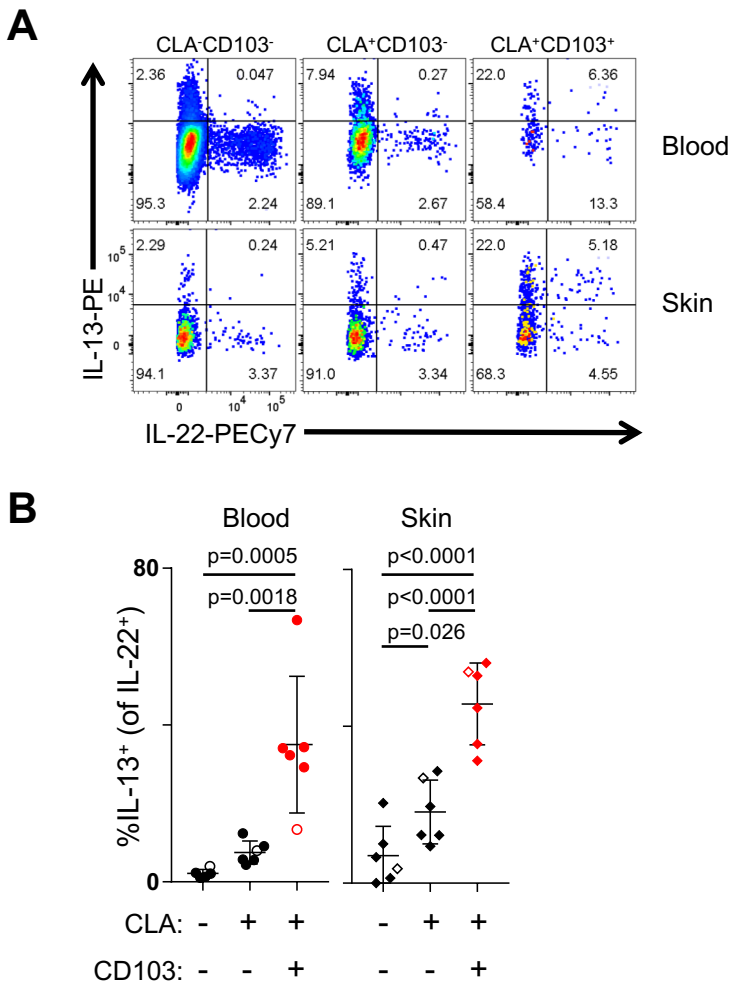

Fig. S7: CLA$^+$CD103$^+$ T cells from human blood and skin coproduce IL-22 and IL-13. (**A**) Representative flow cytometry analysis of IL-22 and IL-13 production by the indicated populations of CD4$^+$CD45RA$^-$ T cells from paired blood and skin following PMA/ionomycin stimulation. (**B**) Graphical summary of the proportion of IL-13$^+$ cells among IL-22$^+$ CLA$^-$ CD103$^-$, CLA$^+$CD103$^-$ and CLA$^+$CD103$^+$ CD45RA$^-$ memory T cells as indicated in blood and skin. Open symbols represent data from a subject with mammary carcinoma. Significance determined by one-way repeated measures ANOVA with Tukey's post-test for pairwise comparisons.

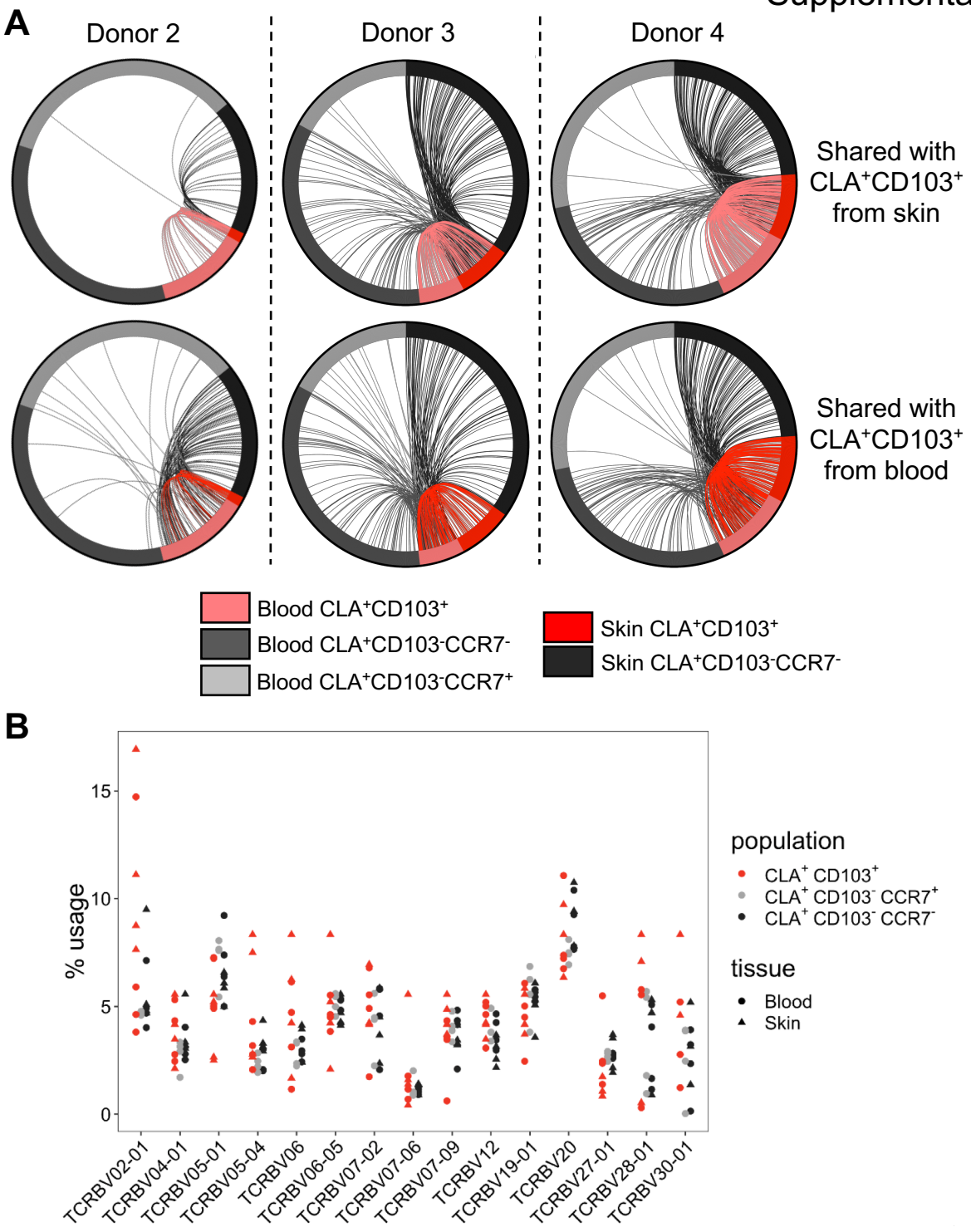

Fig. S8: Analysis of TCRβ repertoire overlap and Vβ gene usage in CLA⁺ T cells from blood and skin. (**A**) Circle plots of unique productive TCRβ sequences from each of the indicated populations of CLA⁺ T cells from each donor examined. Connections highlight sequences from blood or skin CLA⁺CD103⁺ cells found in each of the other populations as indicated. For visualization, sequences were downsampled (weighted for relative abundance) for populations containing >1000 unique sequences. (**B**) Graphical analysis of TCR Vβ segment usage in the indicated populations from across all four donors examined. The plot includes V gene segments that have a usage ≥5% in at least one sample.

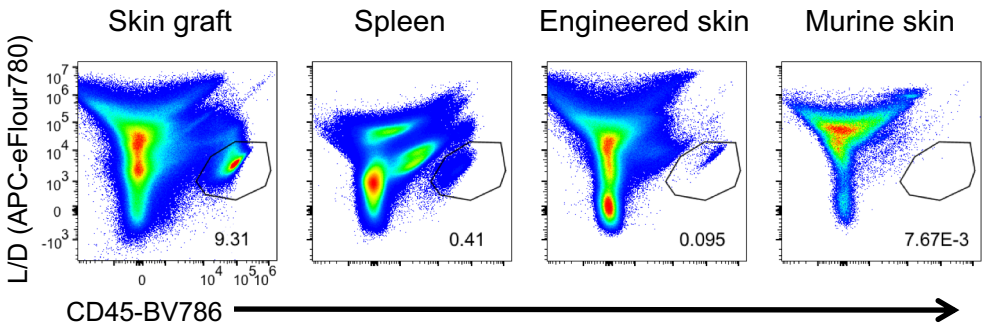

Fig. S9: Human skin-derived cells do not infiltrate murine skin. Representative flow cytometry analysis of human CD45 expression versus live/dead stain of cells isolated from full-thickness skin graft, spleen, engineered skin, and adjacent murine skin 5 weeks after skin grafting.

	Total T cell numbers	**% $CD4^+$ T cells of $CD3^+$**	**$CD103^+CLA^+$ T cells of $CD4^+$**		**% of total CLA^+CD103^+ cells**
			%	#	
Blood	1.1×10^{10}	72.13	0.13	10,314,590	**0.6**
Skin	2.04×10^{10}	57.54	13.74	1,612,823,184	**99.4**

Table S1: CLA^+CD103^+ T cells in circulation constitute a minor fraction of all CLA^+CD103^+ T cells. Calculation of CLA^+CD103^+ T cell numbers in skin and blood were based on total T cell numbers in these tissues as determined in reference *(13)*, the average frequency of $CD4^+$ T cells in each tissue as determined by the investigator's labs, and the average frequency of $CD103^+CLA^+$ T cells in each tissue as shown in Supplementary Figure 4.

Table S2: Detailed list of antibodies and reagents

Tissue preparation

Reagent	Company	Catalog number
Collagenase Type 4	Worthington	LS004186
DNAse	Sigma-Aldrich	DN25
RPMI 1640	Gibco	31870074
human serum	Sigma-Aldrich	H5667/H4522
Penicillin/streptavidin	Sigma-Aldrich	P0781
L-Glutamine	Gibco	A2916801
NEAA	Gibco	11140035
Sodium-Pyruvat	Sigma-Aldrich	S8636
b-Mercaptoethanol	Gibco	31350-010
PBS	Gibco	14190169
Ficoll Paque Plus	GE-Healthcare	GE17-1440-02

Cellular activation

Reagent	Company	Catalog number
CD4 microbeads	Miltenyi	130-045-101
Immuno Cult Human CD3/CD28 T cell activator	Stemcell Technologies	10971
PMA	Sigma-Aldrich	P8139
Ionomycin	Sigma-Aldrich	I06434
Brefeldin A	Sigma-Aldrich	B6542
Cytofix/Cytoperm kit	BD	RUO 554714
Recombinant human IL-2	Immunotools	11340023

Skin cell culture and transplantation

Reagent	Company	Catalog number
Epilife	Gibco	MEPICF500
DMEM	Gibco	11960-044
MEM	Gibco	11380037
TrypLE express	Gibco	12604021
Primocin	invitrogen	ant-pm-1
Histoacryl	BRAUN	1050044

Tissue preparation from mice

Reagent	Company	Catalog number
BD Pharm Lyse	BD	555899
Collagenase from Clostridium histolyticum	Sigma-Aldrich	C9407
Hyaluronidase	Sigma-Aldrich	H3506

CyTOF

Reagent	Company	Catalog number
PBS (Ca and Mg free)	Sigma	D8537
Cisplatin, 100 mM in DMSO	Enzo Life Sciences	ALX-400-040-M250
Human TruStain FcX	BioLegend	422302
MaxPar Nuclear Antigen Staining Buffer Set	Fluidigm	201063
MaxPar Fix and Perm Solution	Fluidigm	201067
Cell-ID Intercalator-Ir, 125 uM (500X)	Fluidigm	201192A
MaxPar EQ Four Element Calibration Beads	Fluidigm	201078

Histology

Reagent	Company	Catalog number
TissueTek O.C.T. Compound	Sakura	TTEK
Hemalum solution acid acc. to Mayer	Carl Rorth	T865.1
Eosin Y aqueous solution	Sigma	HT110232
ProLong™ Gold Antifade Mountant with DAPI	Invitrogen	P36931

Antibodies

Reagent	Company	Catalog number
CLA FITC (HECA-452)	Biolegend	321306
CLA bv605 (HECA-452)	BD	563960
CD103 APC (Ber-ACT8)	Biolegend	350216
CD103 PE (Ber-ACT8)	Biolegend	350206
CD103 FITC (B-Ly7)	eBioscience	11-1038-42
CD3 BV421 (UCHT1)	Biolegend	300434
CD3 PE (HIT3a)	BD	561803
CD3 PE-Cy5.5 (UCHT1)	eBioscience	15-0038-42
CD4 PE-594 (RPA-T4)	Biolegend	300548
CD4 PE-Cy5 (RPA-T4)	BioLegend	300510
CD4 Alexa Fluor 700 (RPA-T4)	Biolegend	300526
CD8 Pacific Orange (3B5)	eBioscience	MHCD0830
CD8 bv510 (RPA-T8)	Biolegend	301048
CD8 bv785 (RPA-T8)	BioLegend	301046
CD9 PE (M-L13)	BD	341647
CD25 PE-Cy7 (BC96)	eBioscience	302612
CD27 PE-594 (M-T271)	BioLegend	356422
CD27 BV711 (M-T271)	BioLegend	356430
CD45 BV785 (HI30)	Biolegend	304048
CD45RA Alexa Fluor 700 (HI100)	Biolegend	304120
CD69 BV605 (FN50)	Biolegend	310938
CD101 PerCP-Cy5.5 (BB27)	Biolegend	244438
CD127 PE-Cy7 (A019D5)	BioLegend	351320
CD127 bv 421 (HIL-7R-M21)	BD	560823

CCR4 PerCP-Cy5.5 (L291H4)	Biolegend	359406
CCR8 PE (L263G8)	Biolegend	360604
CD45RA PE-e610 (HI100)	eBioscience	61-0458-42
CCR6 PE-Cy7 (R6H1)	eBioscience	25-1969-42
CXCR3 bv421 (1C6/CXCR3)	BD	562558
CCR6 PE-Cy7 (G034E3)	Biolegend	353418
CCR7 bv421 (G043H7)	BioLegend	353232
CCR7 bv605 (G043H7)	Biolegend	353224
IFN-g BV605 (4S.B3)	BD	563731
IL-17A PerCP-Cy5.5 (eBio64DEC17)	eBioscience	45-7179-42
IL-13 PE (JES10-5A2)	BD	554571
IL-22 PE-Cy7 (22URTI)	eBioscience	25-7229-42
GM-CSF bv421 (BVD2-21C11)	BD	562930
Fixable Viability Dye eFluor® 780	eBioscience	65-0865-14
TCRgd PerCP-eFluor710 (B1.1)	eBioscience	46-9959
IF primary antibody: rabbit anti-human NC-1 domain of type VII collagen (LH7.2)	kindly provided by Dr. Alexander Nyström, University of Freiburg, Germany	
IF secondary antibody: goat anti-rabbit A488	ThermoFisher	A11008
mLy6G (Gr-1) InVivoMab RB6-8C5	BioXcell	BE0075

Antibodies for CyTOF

Reagent	Company	Catalog number
CLA FITC (HECA-452)	BioLegend	321306
Integrin-beta7 APC (FIB504)	BioLegend	321208
CTLA4 147Sm (14D3)	Fluidigm	Custom
Ki-67 161Dy (B56)	Fluidigm	3161007B
Foxp3 162Dy (259D/C7)	Fluidigm	3162024A
CCR6 141Pr (G034E3)	Fluidigm	3176022A
CD19 142Nd (HIB19)	Fluidigm	3142001B
CD123 143Nd (6H6)	Fluidigm	3143014B
CD38 144Nd (HIT2)	Fluidigm	3144014B
CD4 145Nd (RPA-T4)	Fluidigm	3145001B
IgD 146Nd (IA6-2)	Fluidigm	3146005B
CD16 148Nd (3G8)	Fluidigm	3148004B
CCR4 149Sm (205410)	Fluidigm	3149029A
CD103 151Eu (Ber-ACT8)	Fluidigm	3151011B
CD45RO 152Sm (UCHL1)	Fluidigm	Custom
CD45RA 153Eu (HI100)	Fluidigm	3153001B
CD45 154Sm (HI30)	Fluidigm	3154001B
CD27 155Gd (M-T271)	Fluidigm	3155001B
CXCR3 156Gd (1C6)	Fluidigm	3156004B
CD10 158Gd (HI10a)	Fluidigm	3158011B
CD161 159Tb (HP-3G10)	Fluidigm	3159004B
CD14 160Gd (M5E2)	Fluidigm	3160001B
Anti-APC 163Dy	Fluidigm	3163001B
CCR0 164Dy (314305)	Fluidigm	Custom
CD127 165Ho (A019D5)	Fluidigm	3165008B
CD24 166Er (ML5)	Fluidigm	3166007B
CCR7 167Er (150503)	Fluidigm	3167009A
CD8 168Er (SK1)	Fluidigm	3168002B
CD25 169Tm (M-A251)	Fluidigm	3169003B
CD3 170Er (UCHT1)	Fluidigm	3170001B
IgM 172Yb (MHM-88)	Fluidigm	3172004B
HLA-DR 173Yb (L243)	Fluidigm	3173005B
Anti-FITC 174Yb	Fluidigm	3174006B
CRTh2 175Lu (BM16)	Fluidigm	Custom
CD56 176Yb (HCD56)	Fluidigm	3176001B